Article

Cell

Nuclear Pore Permeabilization Is a Convergent Signaling Event in Effector-Triggered Immunity

Graphical Abstract

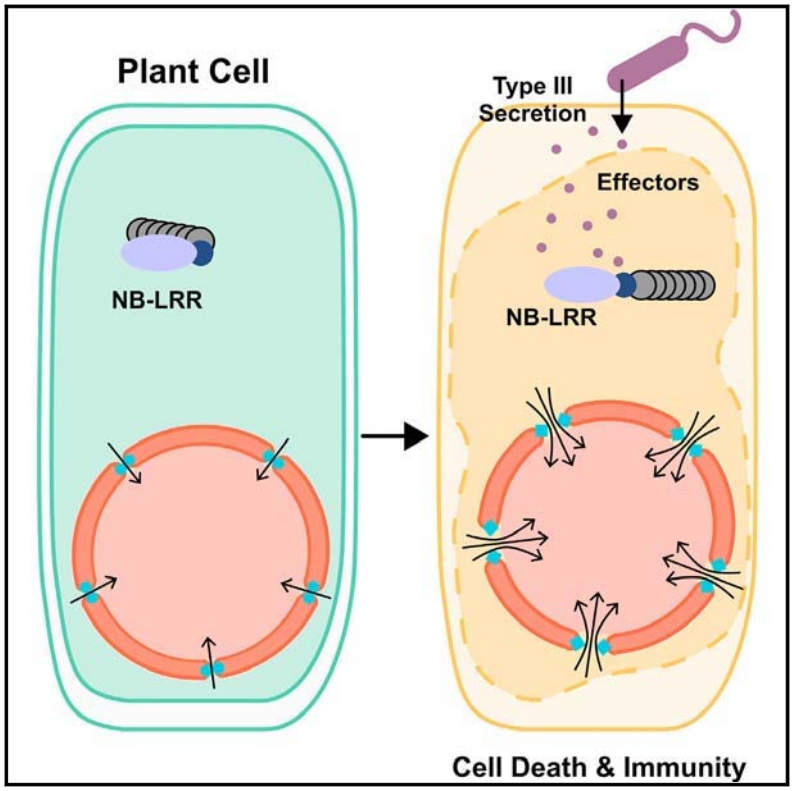

Authors

Yangnan Gu, Sophia G. Zebell, Zizhen Liang, Shui Wang, Byung-Ho Kang, Xinnian Dong

Correspondence

xdong@duke.edu

In Brief

Rather than being a passive conduit, the nuclear pore complex, in response to immune signals, undergoes a conformational switch to reconfigure the selective barrier and promote stress signaling.

Highlights

- CPR5 is a component of the nuclear pore complex (NPC)
- CPR5 regulates nuclear transport through the selective barrier of the NPC
- The CPR5 homomer is disrupted upon induction of effector-triggered immunity (ETI)
- Conformational change in CPR5 leads to CKI release and NPC permeabilization for ETI

Data Resources

GSE72742
GSE72743

Gu et al., 2016, Cell *166*, 1–13
September 8, 2016
http://dx.doi.org/10.1016/j.cell.2016.07.042

CellPress

Please cite this article in press as: Gu et al., Nuclear Pore Permeabilization Is a Convergent Signaling Event in Effector-Triggered Immunity, Cell (2016), http://dx.doi.org/10.1016/j.cell.2016.07.042

Nuclear Pore Permeabilization Is a Convergent Signaling Event in Effector-Triggered Immunity

Yangnan Gu,[1] Sophia G. Zebell,[1] Zizhen Liang,[2] Shui Wang,[3] Byung-Ho Kang,[2] and Xinnian Dong[1,4,*]

[1]Department of Biology, Howard Hughes Medical Institute-Gordon and Betty Moore Foundation, P.O. Box 90338, Duke University, Durham, NC 27708, USA

[2]School of Life Sciences, Center for Cell and Developmental Biology and State Key Laboratory of Agrobiotechnology, The Chinese University of Hong Kong, Hong Kong, China

[3]Development Center of Plant Germplasm Resources, College of Life and Environmental Sciences, Shanghai Normal University, Shanghai 200234, China

[4]Lead Contact

*Correspondence: xdong@duke.edu

http://dx.doi.org/10.1016/j.cell.2016.07.042

SUMMARY

Nuclear transport of immune receptors, signal transducers, and transcription factors is an essential regulatory mechanism for immune activation. Whether and how this process is regulated at the level of the nuclear pore complex (NPC) remains unclear. Here, we report that CPR5, which plays a key inhibitory role in effector-triggered immunity (ETI) and programmed cell death (PCD) in plants, is a novel transmembrane nucleoporin. CPR5 associates with anchors of the NPC selective barrier to constrain nuclear access of signaling cargos and sequesters cyclin-dependent kinase inhibitors (CKIs) involved in ETI signal transduction. Upon activation by immunoreceptors, CPR5 undergoes an oligomer to monomer conformational switch, which coordinates CKI release for ETI signaling and reconfigures the selective barrier to allow significant influx of nuclear signaling cargos through the NPC. Consequently, these coordinated NPC actions result in simultaneous activation of diverse stress-related signaling pathways and constitute an essential regulatory mechanism specific for ETI/PCD induction.

INTRODUCTION

Effector-triggered immunity (ETI) is a vital mechanism for host recognition of pathogen virulence effectors to trigger defense (Jones and Dangl, 2006; Stuart et al., 2013). In plants, ETI is activated by nucleotide-binding leucine-rich repeat (NB-LRR) receptors, which are divided into two major classes based on the presence of an N-terminal coiled-coil (CC) domain or a Toll-interlukin1 receptor (TIR) domain. NB-LRRs have been found to localize in various subcellular compartments, where they can detect activities of different pathogen effectors (Elmore et al., 2011). Although quantitative differences exist in outcomes of ETI mediated by different NB-LRRs, they all result in similar transcriptional reprogramming of the infected cells, which leads to restriction of pathogen growth and rapid programmed cell death (PCD). This suggests a common cellular regulatory mechanism connecting distinct NB-LRR activation events to a unified transcriptional response in the nucleus.

Genetic and molecular studies have shown that changes in the nucleocytoplasmic dynamics of NB-LRR receptor complexes, signal transducers, and immune-related transcriptional regulators are crucial for defense gene expression and resistance during ETI (García and Parker, 2009; Rivas, 2012). Screens for suppressors of an autoactivated TIR-NB-LRR protein mutant, *snc1*, led to the identification of *mos* (*modifiers of snc1*) mutants, including two (*mos3* and *mos7*) in the nuclear pore complex (NPC) and one (*mos6*) in a nuclear transport receptor (NTR) (Cheng et al., 2009; Palma et al., 2005; Zhang and Li, 2005). This and other evidence suggests that the NPC- and NTR-directed nucleocytoplasmic transport is involved in subcellular defense coordination triggered by NB-LRRs (Wirthmueller et al., 2013). However, because these *mos* and other nucleoporin mutants are also compromised in resistance independent of NB-LRRs (Wiermer et al., 2012), whether the NPC plays a generic role in mediating transport of defense signals or a specific regulatory role for distinct immune mechanisms remains unclear.

In contrast to the *mos* mutants, which block immune responses, loss-of-function mutations in the putative nuclear envelope (NE) protein constitutive expresser of PR genes 5 (CPR5) result in an ETI-like transcriptome and PCD (Wang et al., 2014). Consequently, these mutants show resistance against multiple pathogens carrying effectors independent of cognate NB-LRR receptors (Boch et al., 1998; Bowling et al., 1997). This evidence suggests that CPR5 regulates an essential downstream inhibitory mechanism of ETI/PCD, possibly at the nucleocytoplasmic barrier.

We previously showed that two cyclin-dependent kinase inhibitors (CKIs), SIAMESE (SIM), and SIAMESE-related 1 (SMR1), are redundantly required for downstream ETI/PCD signaling in the *cpr5* mutant. CPR5 sequesters CKIs in the NE and specifically releases them in response to NB-LRR activation to engage the retinoblastoma (Rb) and the E2F-mediated cell-cycle pathway to regulate defense gene expression and PCD (Wang et al., 2014). However, how CKIs are released remains unknown. Moreover, whether redirection of the cell-cycle

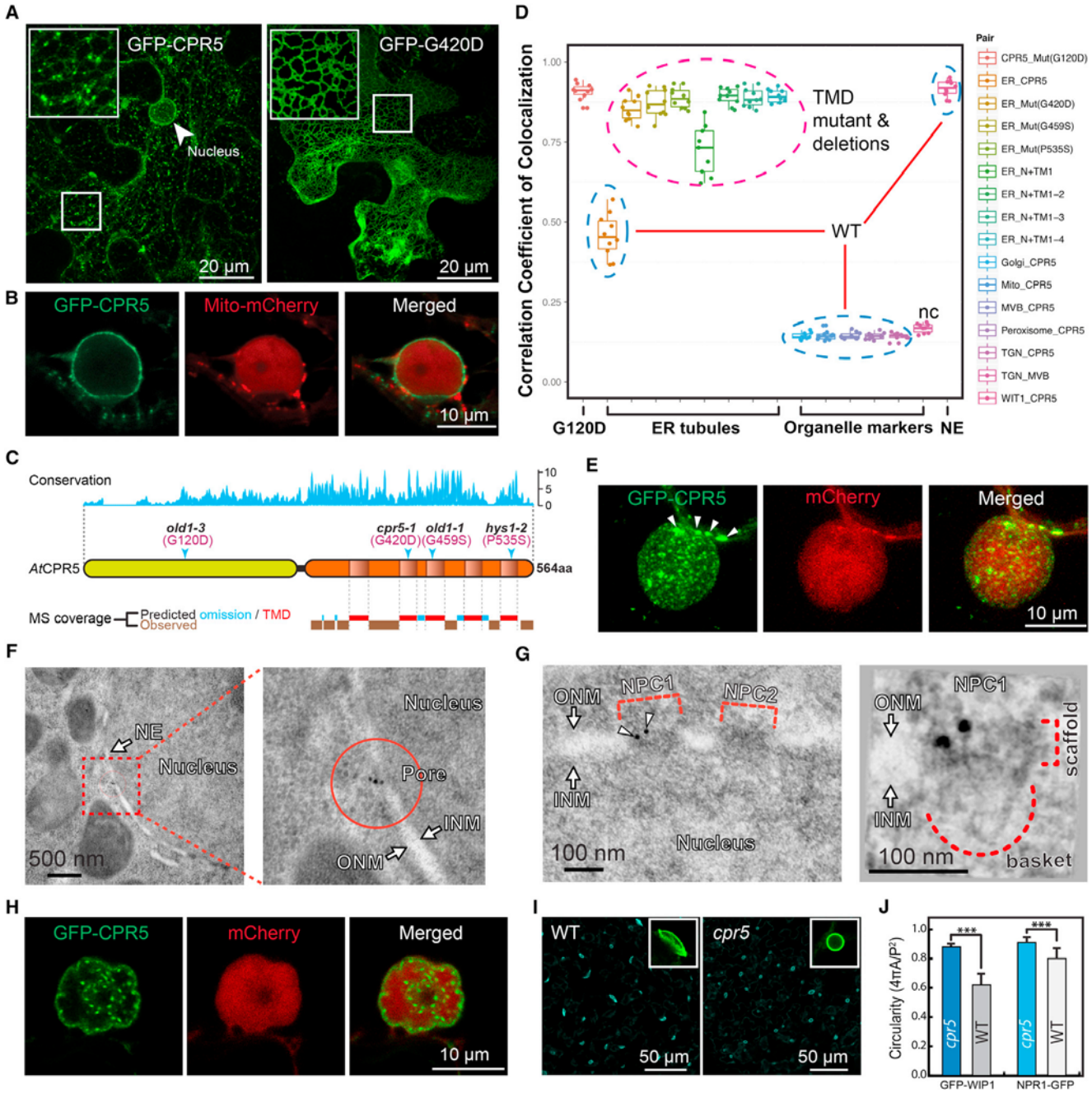

Figure 1. CPR5 Is a Transmembrane Protein Enriched in the Nuclear Pore

(A and B) Subcellular localization of GFP-tagged CPR5 when transiently expressed in *N. benthamiana*. Wild-type (WT) CPR5 (A, left), the G420D mutant (A, right), and WT CPR5 co-expressed with a mCherry-tagged marker labeling mitochondria and nucleoplasm (B) were shown. Images were obtained 24 hr post *Agrobacterium* infiltration.

(C) CPR5 contains an evolutionarily conserved transmembrane (TM) region at the carboxyl terminus. Top: amino acid conservation map derived from multiple sequence alignments of CPR5 proteins from *Micromonas pusilla*, *Chlorella variabilis*, *Physcomitrella patens*, *Sorghum bicolor*, *Selaginella moellendorffii*, *Vitis vinifera*, *Populus tricocarpa*, *Ricinus communis*, *Oryza sativa*, *Zea mays*, and *Arabidopsis thaliana*. Middle: schematic of AtCPR5 domain structure with transmembrane TM domains (TMDs) predicted by TMpred. Arrowheads indicate sites of loss-of-function missense mutations. Bottom: liquid chromatography-tandem mass spectrometry (LC-MS/MS) peptide coverage in the C-terminal half of AtCPR5 purified from transgenic *Arabidopsis*. Predicted omissions were calculated by PeptideMass for trypsin digestion (see Figure S1C).

(D) Pearson's correlation coefficients of co-localization between CPR5 and endomembrane organelle markers. WT CPR5 (blue dashed circles) co-localized with both the nuclear envelope (NE) marker (WIT1) and ER-associated granules (see Figure S1B). CPR5 with missense mutations in the TMDs (Mut) and sequential truncations of individual TMDs (N + TM) all exclusively localized in tubular ER structures (magenta dashed circle). TGN (early endosome) and MVB (late endosome) markers were used as a negative control (nc).

(legend continued on next page)

pathway is sufficient for *cpr5*-mediated ETI/PCD needs further investigation.

In this study, we report that CPR5 is a plant transmembrane nucleoporin that physically associates with the NPC core scaffold. CPR5 resides in the NPC as a homomeric complex, which is specifically disrupted in response to NB-LRR activation. This conformational change in the NPC plays a dual role during ETI/PCD activation: it enables dissociation of CKIs from the NPC to engage cell-cycle regulators for defense gene expression and reconfigures the NPC selective barrier to allow massive nuclear influx of diverse stress-related signaling cargos. These CPR5-coordinated actions of the NPC are required for ETI/PCD induction and constitute a downstream regulatory mechanism specific for NB-LRR-mediated ETI/PCD.

RESULTS

CPR5 Is a Transmembrane Protein Enriched in the Nuclear Pore

To define the molecular role of CPR5, we first determined its precise subcellular localization using a fusion to the GFP (GFP-CPR5), which we have previously shown to be functional (Wang et al., 2014). Using both transient expression in *Nicotiana benthamiana* and stable expression in *Arabidopsis*, we found that CPR5 was exclusively associated with the endomembrane system, including the nuclear envelope (NE) and endoplasmic reticulum (ER)-associated large granules (Figures 1A, 1B, S1A, and S1B). We next investigated its membrane targeting mechanism by first verifying its predicted transmembrane domains (TMDs). Using trypsin digestion followed by shotgun sequencing with mass spectrometry (MS), we found a highly biased peptide coverage pattern. In the conserved C-terminal region of AtCPR5, no peptide was detected within the predicted TMDs (Figures 1C and S1C), consistent with the MS profiling patterns found in other integral membrane proteins (Washburn et al., 2001). Null mutations within the TMDs (Anderson, 2006; Jing et al., 2007; Yoshida et al., 2002) (Figure 1C) and sequential deletions of TMDs from the C-terminal end all caused the protein to be trapped in a tubular ER structure (Figures 1A, right panel, and 1D), highlighting the importance of these TMDs in functional targeting of the CPR5 protein.

Three-dimensional image reconstruction of the nuclear surface revealed that CPR5 was not distributed evenly in the NE, but was enriched in punctate structures (Figures 1E and S1A, right panel). Distinct from the large mobile granules associated with the ER, these static puncta are smaller in size and densely distributed in the NE, resembling nuclear pores. Subsequent immunogold labeling of GFP-CPR5 followed by transmission electron microscopy (TEM) and tomography analyses confirmed that CPR5 is indeed associated with the NPC (Figures 1F and 1G). Structural integrity of the NPC is known to play a role in maintaining NE stability (Alber et al., 2007) and changes in levels of a number of NPC components (nucleoporins) cause NE membrane deformation (Jevtić et al., 2014). We found that prolonged overexpression of CPR5 could indeed elicit hypolobulated nuclei and inner nuclear speckles (Figure 1H), whereas loss of CPR5 resulted in abnormal spherical nuclei (Figures 1I and 1J), consistent with the NE morphology observed in multiple nucleoporin mutants (Parry, 2014; Parry et al., 2006; Tamura et al., 2010). In contrast to its NE localization, which clearly has a functional impact, CPR5-associated ER granules are distinct from any of the known membrane structures tested (Figures 1D and S1B). We hypothesize that this pool of CPR5 may represent a non-specific membrane association due to overexpression.

CPR5 Is a Transmembrane Nucleoporin Associated with the NPC Core Scaffold

Proteomic analysis of the affinity-purified YFP-CPR5 protein complex identified a total of 28 potential binding partners of CPR5 (Figures S2A and S2B), which contain two functional groups that support our hypothesis of CPR5 being a membrane-bound nucleoporin (Figure 2A). The first group contains proteins that function in membrane protein synthesis and maturation. These interactors were likely captured by newly synthesized CPR5 protein in the ER on route to the NE. The second group consists of two proteins, nucleoporin 155 (Nup155), a core scaffold component of NPC, and a putative cell-cycle controlling phosphatase, both of which were previously identified as associated with the NPC in plants (Tamura et al., 2010). We subsequently verified that CPR5 and Nup155 interact specifically in the NPC using the bimolecular fluorescence complementation (BiFC) assay (Figure 2B). In addition, a fluorescence recovery after photobleaching (FRAP) assay indicated that CPR5 is anchored in the NE with low mobility and thus likely forms a stable complex with Nup155 in the NPC (Figure 2C).

To gain further insight into the position of CPR5 within the NPC, we mapped the interactions of CPR5 with nucleoporins of different NPC subcomplexes. The core NPC contains eight copies of symmetric spokes, each consisting of interconnected subcomplexes: the outer ring complex (ORC) that coats the pore membrane, the inner ring complex (IRC) that forms the NPC core scaffold together with the ORC, the transmembrane ring (MR) that anchors the core scaffold to the pore membrane, and the linker nucleoporins that bridge the core scaffold and Phe-Gly

(E) Three-dimensional image reconstruction of the nuclear surface in a GFP-CPR5 expressing cell. The nucleoplasm is labeled by free mCherry. Arrowheads indicate large ER-associated granules close to the nuclear surface.

(F and G) Immunoelectron microscopy and tomography analyses of GFP-CPR5 in root cells of transgenic *Arabidopsis* (F). Immunogold particles (arrowheads) labeled NPC1 but not NPC2 as antibodies detect only surface-exposed epitopes (G, left). The scaffold and nuclear basket of NPC1 were recognized together with two GFP-CPR5-specific immunogold particles in a projection of the tomographic volume (G, right). ONM/INM, outer/inner nuclear membrane.

(H) Hypolobulated NE and inner nuclear speckles resulted from prolonged overexpression of GFP-CPR5 (40 hr after *Agrobacterium* infiltration).

(I and J) Nuclear morphology in WT and *cpr5* mutant plants. Epidermal cells of 5-day-old seedlings expressing the NE marker GFP-WIP1 were imaged (I). Quantification of the nuclear circularity was performed using GFP-WIP1 and NPR1-GFP as NE and nucleoplasm markers, respectively (J). Data are presented as mean ± SD of the mean (SDM; n = 30 cells for each marker and genotype). Asterisks indicate significance (Student's t test, ***$p < 0.001$).

See also Figure S1.

A

Protein	Norm. FC	*p*-value	Loci	Interolog conf.	Group
CPR5	133	9.4e-07	ER/NPC		
Sec61α	inf.	9.7e-03	ER	None	1
HAP6	15	8.8e-03			
RHD3	inf.	4.6e-02			
TMN3	inf.	3.0e-02			
STT3a	inf.	4.6e-02	Golgi		
Nup155	inf.	4.6e-02	NPC	12 (High >10)	2
AT4G24750	inf.	4.6e-02	NPC		

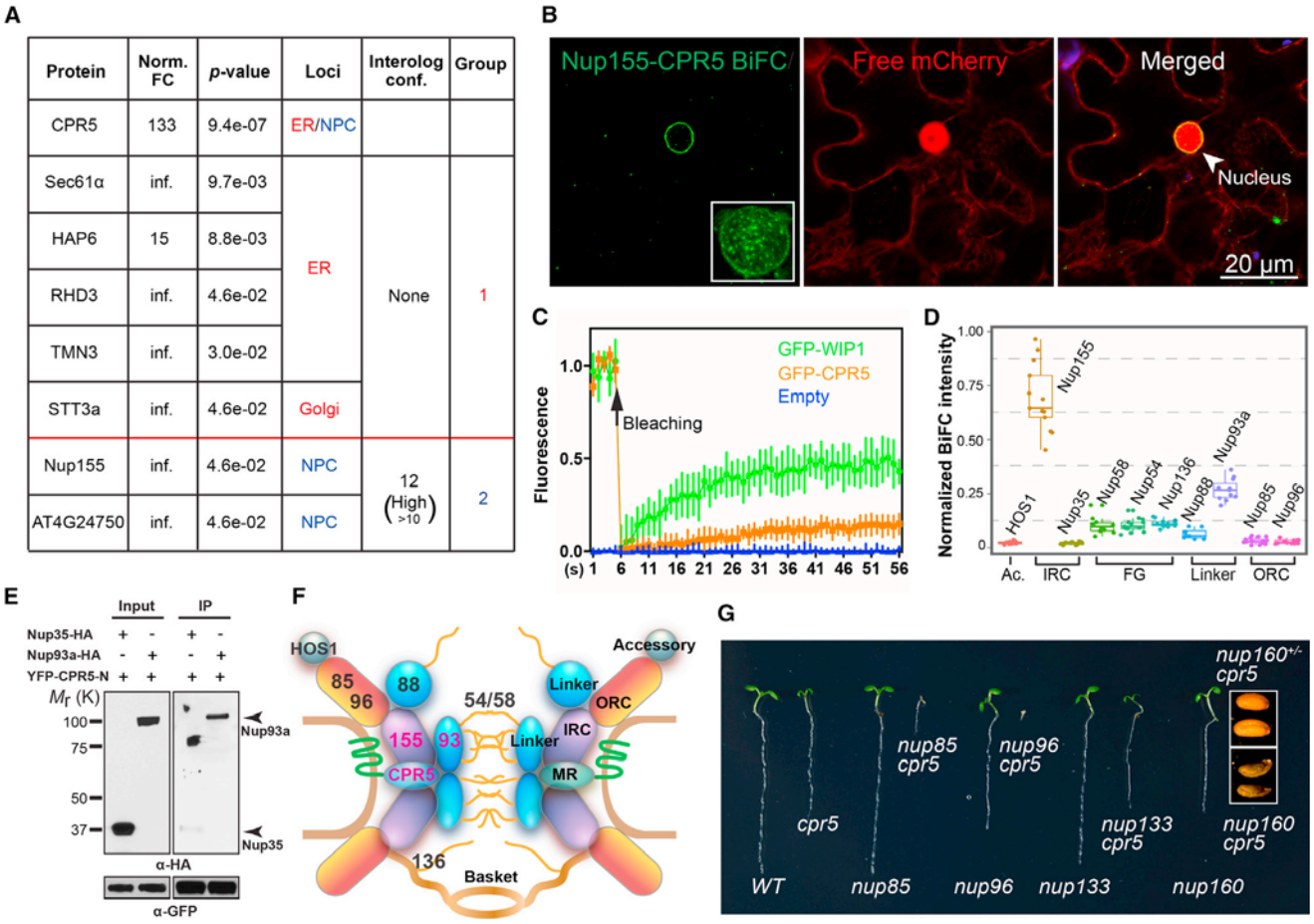

Figure 2. CPR5 Physically and Genetically Interacts with Nucleoporins as a Component of the NPC

(A) CPR5 interactors identified by protein complex purification followed by LC-MS/MS. FC, fold change of spectrum counts in YFP-CPR5 versus GFP sample. Infinite (inf.) indicates that peptide was not detected in GFP samples. Interolog conf., confidence of predicted interaction between proteins.

(B) CPR5 and Nup155 interacts in the NE. Bimolecular fluorescence complementation (BiFC) assay was performed by transiently coexpressing nYFP-CPR5 and Nup155-cYFP in *N. benthamiana*. The interaction pattern on the nuclear surface was reconstructed by z stack images (inset).

(C) Fluorescence recovery after photobleaching (FRAP) analysis of GFP-CPR5 in transgenic *Arabidopsis*. A mobile NE protein GFP-WIP1 served as a control. Data are presented as mean ± SDM (n = 5 experimental replications).

(D) Interaction mapping of CPR5 with nucleoporins. BiFC was performed by transiently coexpressing nYFP-CPR5 with Nup-cYFP in *N. benthamiana*. The BiFC intensity was normalized using averaged expression levels of corresponding Nup-YFP measured in separate experiments. Ac, accessory nucleoporin; IRC, inner ring complex; FG, Phe-Gly repeat-containing nucleoporin; ORC, outer ring complex; Linker, linker nucleoporin.

(E) CPR5 interacts with the IRC-associated linker nucleoporin Nup93a. In vitro pull-down assay was performed using GFP-TrapA agarose beads. YFP-CPR5-N, YFP-tagged N-terminal half of CPR5.

(F) The structural modules of the nuclear pore complex (NPC) and the proposed position of CPR5 within the NPC.

(G) Genetic interaction between *cpr5* and mutants of the ORC nucleoporins. Five-day-old seedlings were shown. Because the *cpr5 nup160* double mutant did not germinate, the seed morphology of the homozygote was compared to that of a heterozygote.

See also Figure S2.

(FG) proteins, which form the selective barrier for cargo transport (Alber et al., 2007). Using both BiFC in planta and an in vitro pull-down assay, we found that CPR5 interacts with not only Nup155 in the IRC but also the IRC-associated linker nucleoporin Nup93a through its N terminus (Figures 2D and 2E). However, no robust interaction was detected with FG proteins, ORC components, or other NPC accessory proteins tested (Figure 2D). Based on these observations, we propose that CPR5 is a transmembrane nucleoporin that is anchored at the equatorial plane of the NPC in the nuclear pore membrane by its C-terminal TMDs and physically interacts with the NPC core scaffold as well as an associated linker nucleoporin through its soluble N terminus (Figure 2F).

CPR5 Is Involved in NPC Function

Consistent with the notion of CPR5 being a nucleoporin, CPR5 displays strong genetic interactions with the ORC nucleoporins Nup85, Nup96, and Nup160, but not Nup133. Whereas the *nup85*, *nup96*, and *nup160* single mutants did not exhibit obvious aberrations in early seedling development, double mutants with *cpr5* all resulted in embryonic or seedling lethality (Figure 2G).

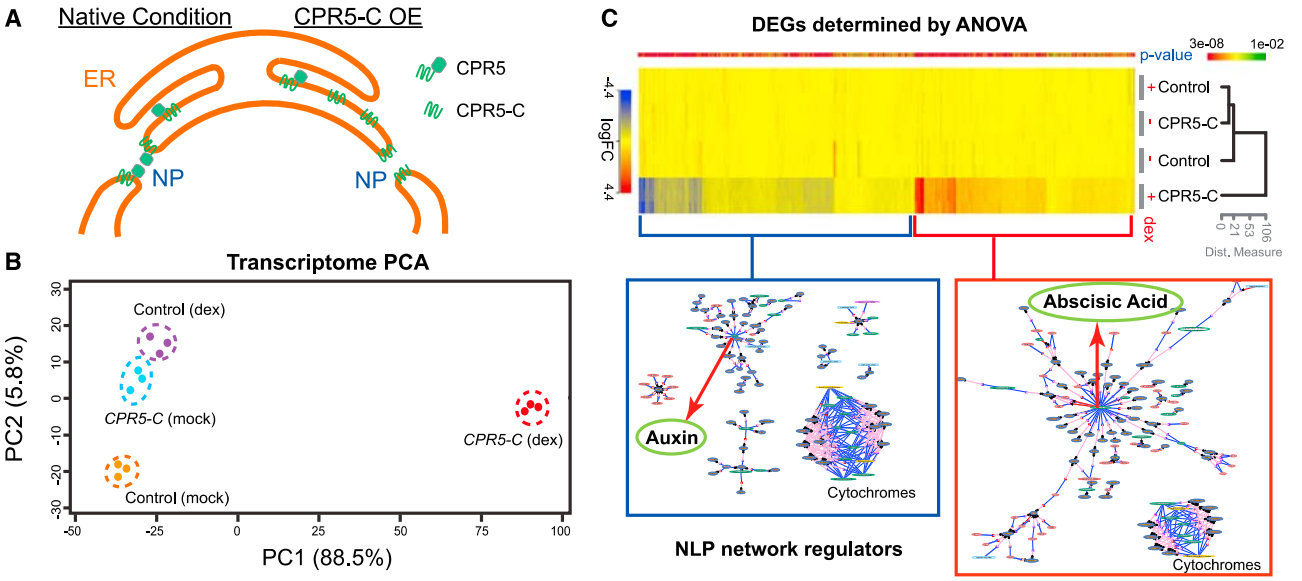

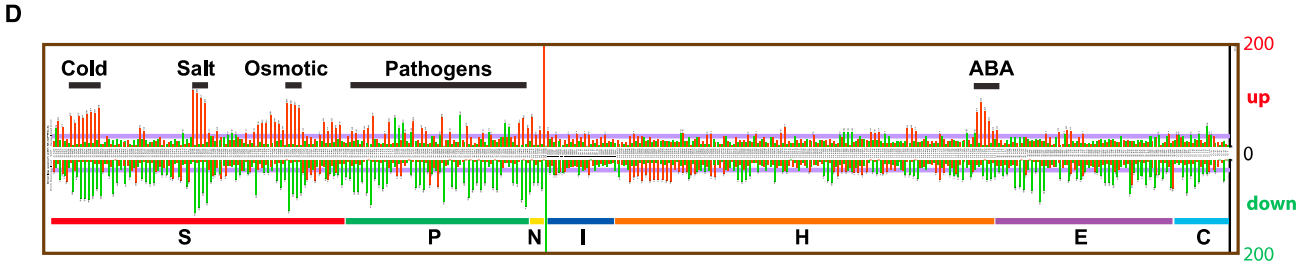

E

Top GSEA coupling-phase match	FDR Up	FDR Down
Dehydration (65% RWC)[a]	2.90e-93	2.71e-60
Autoactive PHYB (YHB)[b]	4.02e-88	1.82e-111
High irradiance (CRY1-dep.)[c]	1.95e-67	7.91e-27
Cold stress (0 °C)[d]	3.02e-38	3.57e-13
DELLA target gene (rga-Δ17)[e]	8.10e-30	2.30e-06
Repressed auxin responses[f]	9.23e-28	4.56e-50

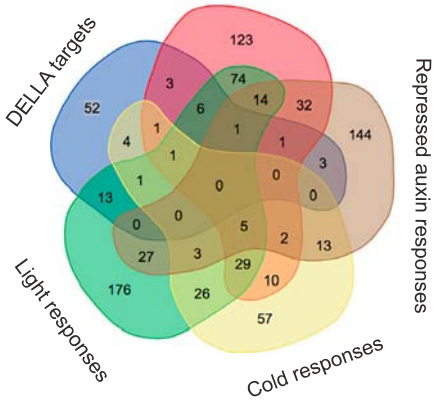

G

Enriched cis-element	p-value
ABRE	<10e-10
G-box motif	<10e-10
Z-box motif	<10e-7
CBF3 binding	<10e-10
GA-down motif	<10e-10
AuxRE	7.8e-05

Figure 3. Transient Interference with CPR5 Function Simultaneously Activates Diverse Nuclear Signaling Pathways

(A) A proposed cellular mechanism for transient interference of CPR5 function by overexpression (OE) of CPR5-C. NP, nuclear pore.

(B) Principal component analysis (PCA) of transcriptome changes induced by transient expression of CPR5-C.

(C) Heatmap of differentially expressed genes (DEGs) that depend on *CPR5-C* transgene induction (p value < 0.01). Genes with fold change (dex versus mock) higher than two were subject to natural language processing (NLP)-based network regulator discovery analysis. Major network regulators are highlighted with red arrows.

(D) Comparative analysis of CPR5-C-mediated CPR5 interference data with 287 published *Arabidopsis* microarrays. Each row represents an analysis with a specific array dataset, and datasets are sub-categorized into sections according to treatments. Section code: S, stress; P, pathogen; N, nutrient; I, inhibitor; H, hormone; E, elicitor; C, chemical. The length of each bar represents the number of overlapping DEGs (up- or downregulated) between the CPR5-C data and a specific treatment.

(E) Gene set enrichment analysis (GSEA). CPR5-C-induced up- and downregulated genes were used as separate inputs for GSEA and non-redundant top matches are listed. PubMed IDs for the listed datasets are: a-21050490, b-19529817, c-17478635, d-16214899, e-17933900, and f-19392692.

(legend continued on next page)

This synergistic genetic relationship is likely due to a cooperative role between CPR5 and ORC components in maintaining the structural integrity of the NPC. We were unable to assess genetic interactions between CPR5 and IRC nucleoporins due to seedling or embryonic lethality of the single mutants (Parry, 2014).

Plants have sequence-homologs of almost all the vertebrate nucleoporins (Tamura et al., 2010). However, because transmembrane nucleoporins are not evolutionarily conserved (Mans et al., 2004), functional analogs of vertebrate transmembrane nucleoporins that interact with the IRC and anchor the NPC to the pore membrane have not been identified in plants. Our study suggests that CPR5 is a plant-specific transmembrane nucleoporin that physically associates with the IRC and may contribute to the stability of the NPC core scaffold even though it is not required for NPC anchoring (Figure S2C). Besides its potential structural role in the NPC, the *cpr5* mutant phenotype suggests that this plant transmembrane nucleoporin may have evolved distinct functions, such as regulation of ETI/PCD.

CPR5 Modulates the Nucleocytoplasmic Transport Activity of the NPC

The NPC is a platform for multiple nuclear activities, including nucleocytoplasmic transport, genome maintenance, and regulation of gene expression (Strambio-De-Castillia et al., 2010). To understand how CPR5 regulates ETI in the NPC, we first investigated the cellular processes controlled by this nucleoporin using transcriptome profiling. To avoid the indirect effects of the stable *cpr5* mutation, which is known to activate ETI as well as the downstream signaling pathways mediated by the immune signal salicylic acid (SA) (Bowling et al., 1997; Wang et al., 2014), a transient interference system was developed. Because of the low turnover rate of nucleoporins (Toyama et al., 2013), we designed a protein interference strategy that involved dexamethasone (dex)-inducible expression of the C-terminal half (275–564 aa) of CPR5 (CPR5-C). Although CPR5-C is not functional (Figure S3A), it is targeted to the NPC (Figure S3B) and therefore might compete with the wild-type (WT) protein (Figure 3A). We first tested the system using a transient expression assay performed in *N. benthamiana*. We found that overexpression of CPR5-C led to tissue collapse similar to ETI-associated PCD induced by NB-LRR activation, whereas overexpression of the full-length CPR5 or CPR5-N had no such an effect (Figure S3C). This CPR5-C-induced PCD was likely due to interference with the function of endogenous CPR5 because it was suppressible by simultaneous overexpression of full-length CPR5, but not CPR5-N (Figure S3D). We subsequently validated the interference activity of YFP-CPR5-C in *Arabidopsis*, where constitutive or inducible expression of YFP-CPR5-C in the WT background resulted in the *cpr5* mutant phenotypes, including growth arrest, PCD and increased expression of defense genes (Figures S3E–S3G).

The stable *Dex:YFP-CPR5-C* transgenic line was then used for transcriptome analysis. Using principal component analysis, we detected a major change in global gene expression 24 hr after YFP-CPR5-C was induced (Figure 3B), when SA-mediated response had yet to occur in this system (Figure S3H). Approximately 1,800 differentially expressed genes (DEGs) were identified (Figure 3C; Table S1). Comparative analysis with 287 published *Arabidopsis* microarray datasets collected under the conditions of a board spectrum of chemical/stress/hormone treatments (Reina-Pinto et al., 2010) revealed that the CPR5-C-induced transcriptome has significant matches with a variety of stress responses, especially to cold, salt/osmotic stress, abscisic acid, and various pathogens (Figure 3D). We also performed gene set enrichment analysis (GSEA) using an even more comprehensive database (Yi et al., 2013), which revealed a transcriptome feature composed of distinct molecular signatures, including activation of cold/dehydration/ABA responses and PHYB/CRY1-dependent light responses, and repression of gibberellin and auxin responses (Figures 3E and 3F). The significance of these molecular signatures was further supported by the enrichment of *cis*-elements known for these responses in total DEGs (Figure 3G).

Such a composite transcriptome profile is most likely due to perturbation of a key cellular process shared by these corresponding pathways instead of crosstalk effects induced by a single signaling pathway. Nucleocytoplasmic protein transport is a critical rate-limiting step for hormones and light signal transduction. Nuclear translocation of photoreceptors PHYs and CRY1 is required for activation of light responses, whereas nuclear accumulation of DELLA and Aux/IAA proteins results in repression of gibberellin and auxin signaling, respectively (Lee et al., 2008). Notably, a number of mutants with altered responses to cold, drought/ABA, and auxin have been genetically identified as components of the NPC and NTRs (Dong et al., 2006; Lee et al., 2001; Parry et al., 2006; Verslues et al., 2006), illustrating the sensitivity of these processes to the structural integrity and/or transport activity of the nuclear pore. Indeed, ABA and auxin were the most sensitive pathways detected by a natural language processing (NLP)-based network regulator discovery algorithm when applied to the DEGs caused by CPR5-C interference (Figure 3C). We hypothesize that with compromised CPR5 function, the NPC adopts a structure with significantly increased permeability and/or transport activity that allows deregulated nuclear influx of diverse signaling cargos, which normally undergo nuclear translocation only under stimulus-induced conditions.

We next tested whether the WT CPR5 constrains the nuclear accumulation of signaling cargos. We found that overexpressing CPR5 indeed caused substantial cytoplasmic retention of stress- and hormone-related nuclear proteins NPR1, JAZ1, and ABI5 (Figures 4A, 4B, S4A, and S4B). However, WIT1 (an NE protein), Nup155 or a mutant form of CPR5 (G420D) could not recapitulate this effect (Figures 4A, S4A, and S4B), supporting a direct role for CPR5 in modulating nucleocytoplasmic transport activity of the NPC. Consistent with the cytoplasmic retention of these nuclear signaling molecules, overexpression

(F) Venn diagram of the transcriptome signatures identified in (E).

(G) Cis-element enrichment analysis of CPR5-C-induced total DEGs. ABRE, ABA-responsive element; G/Z-box, light-responsive elements; CBF3, transcription factor for cold acclimation; GA-down, gibberellin downregulated d1 cluster; AuxRE, auxin response element.

See also Figure S3 and Table S1.

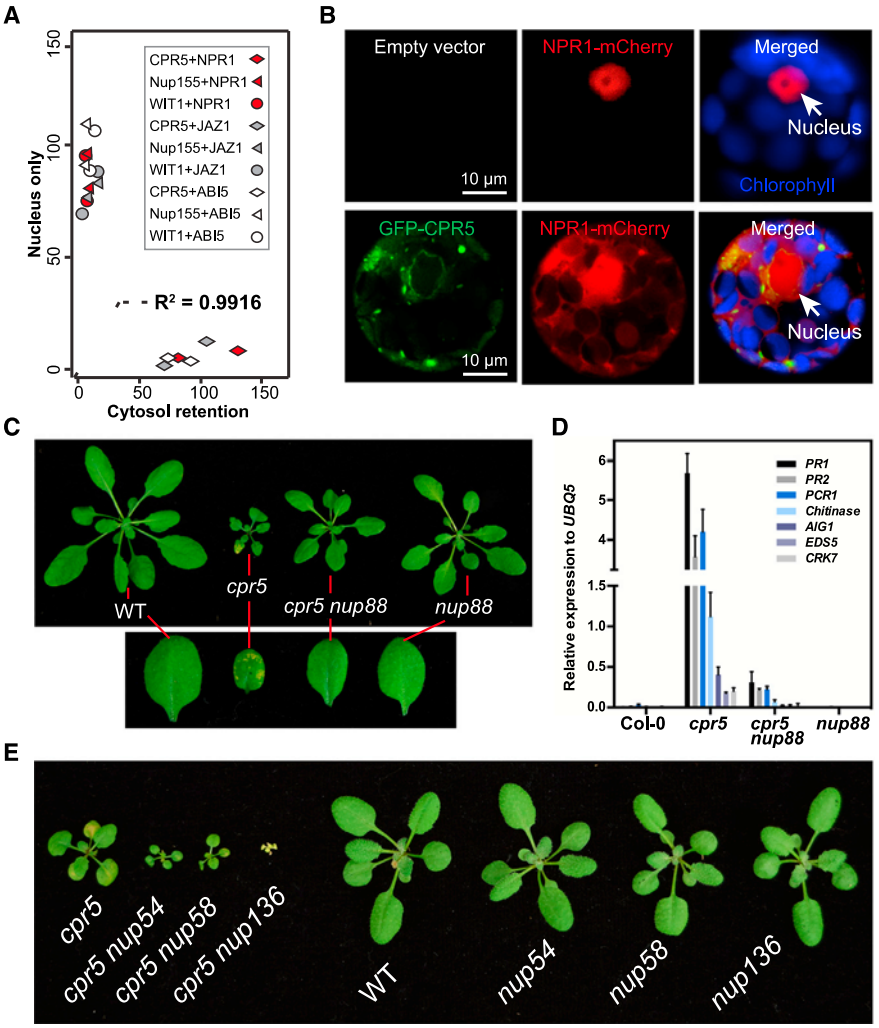

Figure 4. CPR5 Modulates Protein Nucleocytoplasmic Transport to Gate ETI

(A) Overexpression of CPR5 resulted in cytosolic retention of nuclear proteins. NPR1, JAZ1, or ABI5 was co-expressed with NPC protein CPR5, Nup155, or WIT1 in *Arabidopsis* protoplasts. Each combination was repeated twice with ~100 transformed cells counted per repeat. Localization of nuclear proteins in each cell was recorded as binary data ("nucleus only" or "cytosol retention"). A logistic regression model using the NPC protein as the sole independent variable explains 99% of the data variance.

(B) Representative *Arabidopsis* protoplasts co-transformed with NPR1-mCherry and GFP-CPR5 constructs or the empty vector.

(C) Four-week-old WT, *nup88* (also known as *mos7-1*), *cpr5*, and *nup88 cpr5* plants are shown. The lower panel shows close-ups of leaves with or without spontaneous PCD.

(D) Expression levels of the most induced defense-related genes in the *cpr5* mutant were measured using qRT-PCR. Data are presented as mean ± SDM (n = 2 biological replicates).

(E) Three-week-old WT, *cpr5*, *cpr5 nup54*, *cpr5 nup58*, *cpr5 nup136*, *nup54*, *nup58*, and *nup136* plants.

(F) FG-Nup mutants *nup54* and *nup136* specifically enhanced ETI, but not basal immunity. Three-week-old plants were inoculated with bacterial pathogen *Pseudomonas syringae* pv. *maculicola* (*Psm*) without (left) or with (right) the effector gene *AvrRpt2*. Data are presented as mean ± SDM (n = 6 biological replications for each genotype and treatment). Two-way ANOVA was used for statistical tests. *p < 0.05, **p < 0.01, ***p < 0.001, n.s., not significant.

See also Figure S4.

CPR5 compromises ETI-associated PCD and resistance in *Arabidopsis* (Wang et al., 2014), suggesting that CPR5 is a direct rate-limiting regulator for ETI/PCD.

CPR5 Inhibits Immune Signal Transport through the Selective Barrier of the NPC

To further evaluate the functional importance of CPR5-gated NPC cargo transport to ETI/PCD activation and to investigate the gating mechanism, we crossed *cpr5* with stress-related karyopherin mutants as well as transport-related nucleoporin mutants (Figure S4C). We found that a partial loss-of-function mutant of Nup88, which associates with the NPC cytoplasmic filaments, could largely rescue the *cpr5* phenotypes, including the stunted growth, spontaneous PCD, and elevated defense gene expression (Figures 4C and 4D). This mutant has previously been found to block nuclear accumulation of multiple defense-related proteins (Cheng et al., 2009), and its suppressor activity on *cpr5* suggests that NPC-mediated nuclear transport of immune cargos is required for CPR5-gated ETI/PCD activation. In contrast to *nup88*, crossing *cpr5* with mutants of FG nucleoporin *Nup54*, *Nup58*, and *Nup136* exacerbated the *cpr5* phenotype (Figure 4E). More importantly, *Nup54* and *Nup136* display a specific inhibitory role in ETI, as their mutants were found to enhance ETI, but not basal immunity (Figure 4F). This evidence suggests that CPR5 may modulate the properties

of the NPC selective barrier as a mechanism to regulate ETI. Indeed, it has been shown that loss of yeast IRC nucleoporins relaxes the NPC permeability barrier due to inappropriate anchoring of FG nucleoporins (Shulga et al., 2000). Given that CPR5 directly interacts with Nup93 (Figure 2D-2F), the molecular anchor of FG nucleoporins (Chug et al., 2015), we propose that loss-of-CPR5 activates ETI partly by perturbing the structural arrangement of FG meshwork to compromise its inhibitory role in immune signaling cargo transport.

Homomeric Interaction of CPR5 in the NPC Is Required to Inhibit ETI/PCD

Because previous genetic data clearly showed that CPR5 is a negative regulator of ETI/PCD (Boch et al., 1998; Wang et al., 2014), we hypothesize that its repression must be alleviated upon ETI activation. To test this, we first examined, but ruled out, a significant reduction in *CPR5* transcription or translation during ETI triggered by the bacterial pathogen *Pseudomonas syringae* pv. *maculicola* (*Psm*) carrying the effector AvrRpt2 (Figures S5A–S5C). Based on the knowledge that homo- and hetero-oligomerization of nucleoporins is crucial for their functions, we then tested whether CPR5 activity is regulated through homo-oligomerization. We performed BiFC assay in *35S:n/c-YFP-CPR5* transgenic plants coexpressing n-YFP-CPR5 and c-YFP-CPR5 and found that CPR5 indeed formed a homomeric complex in the NE (Figure 5A, left). In a transient assay, the BiFC signal was also observed in the so-called Z-membranes (Figure 5A, right), which are artificial organelles formed when integral membrane proteins oligomerize through their extra-luminal domains (Gong et al., 1996). Because Z-membranes were only observed when n/cYFP were fused to the N terminus of CPR5, we hypothesized that the CPR5 N-terminal domain is extra-luminal and mediates the homomeric interaction (Figure 5B). Indeed, in vitro pull-down assays mapped the homomeric interaction domain to the first two thirds of the CPR5-N (1–274 aa), with the middle region (N2) being essential (Figures 5C–5E and S5D). Notably, a known loss-of-function mutation (G120D, *old1-3*) resides in the CPR5 N2 region (Jing et al., 2007). We found that the G120D mutation significantly compromised CPR5 homomeric interaction (Figures 5F and S5E). Furthermore, at similar protein levels, the monomeric G120D allele could not complement the *cpr5-1* phenotypes as the WT CPR5 (Figure 5G). Because the G120D mutation affected neither CPR5 localization (Figure 1D) nor CPR5 heteromeric interactions with Nup155 and Nup93a (Figure 5H), it appears to specifically affect CPR5 homomeric interaction required for its function.

CPR5 Homomeric Interaction Is Specifically Disrupted upon NB-LRR Immune Receptor Activation

We next investigated how CPR5 homomeric interaction might be regulated upon NB-LRR activation. We introduced the *35S:n/c-YFP-CPR5* into *Arabidopsis* lines carrying a dex-inducible *AvrRpt2* construct in both WT and the cognate immune receptor mutant *rps2* by genetic crosses. We found a significant reduction in the BiFC signal as early as 6 hr after dex provision when the morphology of nucleus (stained by DAPI) was still intact (Figure 6A). This reduction in CPR5 homomeric interaction was dependent on both AvrRpt2 and RPS2 (Figure 6B), but independent of CPR5 protein levels (Figure S5C). Similar results were also obtained in the coimmunoprecipitation experiment using pathogen-challenged *Arabidopsis* plants carrying the *35S:GFP-CPR5* and *35S:HA-CPR5* double transgenes (Figure 6C). A significant reduction in CPR5 homomeric interaction was observed in response to *Psm* carrying AvrRpt2, but not *Psm* without the effector. These results suggest that in response to effector-triggered NB-LRR activation, the CPR5 homomeric complex in the NPC is disrupted to release its inhibition on ETI activation. This hypothesis was supported by comparing the transient CPR5-interference transcriptome described in Figure 3 with time course ETI transcriptional responses mediated by RPS4 (a TIR-NB-LRR) and RPS2 (a CC-NB-LRR). We found that the majority of the genes differentially expressed upon functional interference of CPR5 (Figure 6D, red and blue ovals) overlapped with the transcriptome changes mediated by RPS4 and RPS2 (p value < 1e-50 in both cases) and displayed concordant expression patterns with the ETI response in WT, but not in ETI-deficient *eds1* and *rps2* mutants (Figure 6D). In contrast, those genes had limited overlap with the host transcriptome changes induced by a virulent strain that activates the basal immunity and displayed a random distribution. Last, we showed that overexpression of the monomeric mutant form of CPR5 (G120D) resulted in a *cpr5*-like phenotype in WT plants (Figure 6E), suggesting that disruption of CPR5 homomeric interaction is sufficient to activate ETI/PCD downstream of NB-LRR activation.

Disruption of CPR5 Homomeric Complex Coordinates ETI Signaling by Cell-Cycle Regulators

Our previous study showed that physical association of CPR5 with the CKI, SIM (SIAMESE), is diminished upon *Psm/AvrRpt2* challenge, resulting in activation of a non-canonical pathway involving cell-cycle regulators that contributes to ETI and PCD (Wang et al., 2014). To test whether the interaction between CPR5 and CKIs is regulated by the homomeric interaction of CPR5, we performed an in vitro pull-down assay to examine the affinity of SIM to WT CPR5 and the monomeric G120D mutant. We found that the G120D mutation diminished the protein's affinity to SIM (Figures 6F and S6A). This result suggests that the homomeric CPR5-N is necessary for association with SIM, and disruption of this homomeric interaction results in the release of SIM, allowing it to engage in downstream ETI signaling. Although CKIs are required for ETI signaling, overexpressing SIM is not sufficient for activating ETI/PCD unless the CPR5 function is compromised at the same time (Figure S6B), consistent with our hypothesis that elimination of CPR5's inhibitory activity in nuclear transport is also necessary for ETI/PCD activation.

Nucleoporins have been reported to regulate cell-cycle progression through their effect on expression levels of cell-cycle regulators in mammals (Chakraborty et al., 2008). The direct sequestration of the cell-cycle regulators in the NPC by a transmembrane nucleoporin is a surprising finding, whose significance in basic plant cell biology is currently not known. However, this association allows the NPC to play a dual role in response to ETI induction in redirecting certain cell-cycle regulators for defense gene expression and permeabilizing the NPC transport activity for simultaneous activation of diverse stress-related

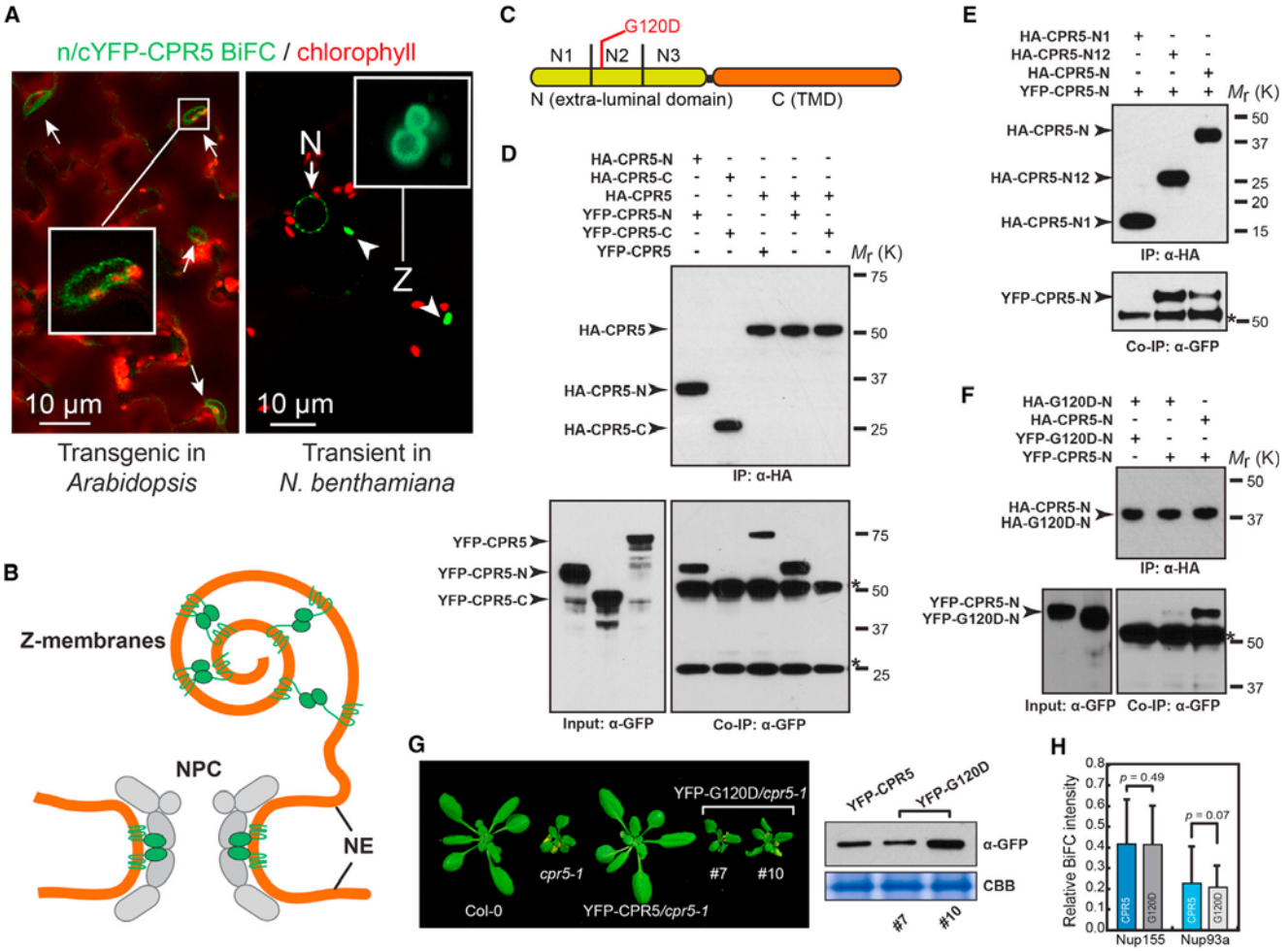

Figure 5. CPR5 Homomeric Interaction at the N-Terminal Extra-Luminal Domain Is Required for Suppressing ETI and PCD

(A) CPR5 BiFC assay. *nYFP-CPR5* and *cYFP-CPR5* were constructed in two separate 35S promoter-driven expression cassettes within one vector (*35S:n/c-YFP-CPR5*). BiFC signals were observed in a stable transgenic *Arabidopsis* line (left) and transiently transformed *N. benthamiana* (right), respectively. Arrows and arrowheads indicate the nucleus and Z-membranes, respectively.

(B) A model proposed for CPR5 homomeric interaction in the NPC and Z-membranes.

(C) Schematic of CPR5 constructs used in in vitro pull-down assays. CPR5-N (1–274 aa) and CPR5-C (275–564 aa). CPR5-N was further divided into N1 (1–91 aa), N2 (92–182 aa), and N3 (183–274 aa).

(D–F) CPR5 homomeric interaction is mediated by its N-terminal extra-luminal domain. CPR5-N, rather than CPR5-C, mediated the homomeric interaction (D). The N1 and N2 (N12) domains of CPR5-C is sufficient and the N2 domain is necessary for the interaction (E). The G120D mutation compromised the homomeric interaction of CPR5-N (F). In vitro pull-down assays were performed using HA antibody-conjugated agarose beads. Stars indicate non-specific signals from immunoglobulins.

(G) Homomeric interaction is required for CPR5 function. *35S:YFP-CPR5* fully complemented the *cpr5-1* mutant phenotype but *35S:YFP-G120D* did not (left) when expressed at comparable levels (right). Two independent *35S:YFP-G120D* transgenic lines (#7 and #10) are shown.

(H) The G120D mutation does not affect heteromeric interactions of CPR5 with other nucleoporins. BiFC was performed by transiently coexpressing nYFP-CPR5/G120D pairwise with Nup155/Nup93a-cYFP in *N. benthamiana*. The BiFC intensity was normalized using averaged expression levels of YFP-CPR5/G120D measured in separate experiments and plotted as relative values. Data are presented as mean ± SDM (n = 15 cells for each BiFC combination). p values were calculated by Student's t test.

See also Figure S5.

nuclear signaling, both of which are necessary for the activation of ETI/PCD in plants (Figure 6G).

DISCUSSION

NPC-dependent nuclear transport of immune receptors, signal transducers, and transcription factors represents a prevalent regulatory mechanism for immune activation in both plants and animals (Deslandes and Rivas, 2011; García and Parker, 2009; Gilmore, 2006; Rivas, 2012). To promote nuclear translocation, protein cargos usually undergo changes in affinity to nuclear transport receptors or piggybacks on molecules with mechanisms for nuclear translocation (Wirthmueller et al., 2013). However, whether the NPC itself has a direct role in immune signaling

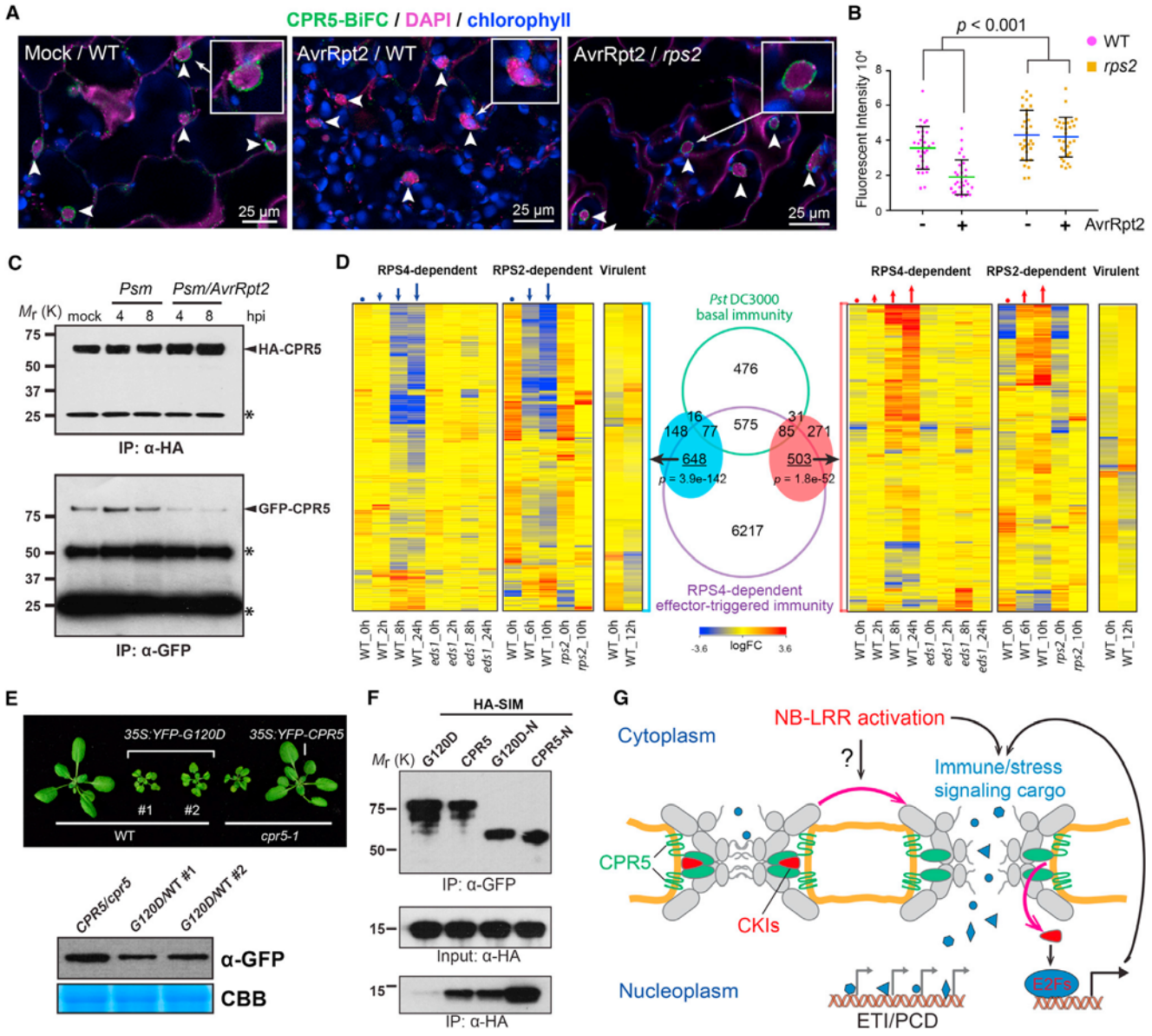

Figure 6. Disruption of CPR5 Homomeric Interaction Is Triggered by NB-LRR Activation and Coordinates CKI-Mediated ETI Signal Transduction and NPC Permeabilization

(A–C) ETI-triggered disruption of CPR5 homomeric interaction in the NPC. Leaves of *35S:n/c-YFP-CPR5/Dex:AvrRpt2* double transgenic line were incubated with mock or 50 μM dex for 6–8 hr before imaging (A). DAPI stained nuclei (arrowheads). BiFC intensities in the NE were measured (B). Data are presented as mean ± SDM (n = 30 cells for each genotype and treatment). Statistical test was performed using two-way ANOVA. Total protein was extract from *35S:GFP-CPR5/HA-CPR5* double transgenic plants treated with *Psm* at indicated time points. Immunoprecipitation was performed using anti-HA agarose beads in the presence of high concentration of detergents (C). hpi, hours post inoculation.

(D) CPR5 interference transcriptome shows a significant overlap and concordant expression pattern with those of ETI. Overlaps between CPR5-C-induced (red oval) and repressed (blue oval) genes with *RPS4*-dependent ETI genes and basal immunity genes are shown in Venn diagram. Hypergeometric tests were used to calculate p values.

(E) *35S:YFP-G120D* caused dominant-negative phenotype in WT plants. Two independent transgenic lines (#1 and #2) and their expression levels are shown.

(F) CPR5 homomeric interaction is required for interaction with SIM. CPR5/G120D was tagged with YFP and SIM was tagged with HA. In vitro pull-down assay was performed using GFP-TrapA beads.

(G) Permeabilization of the NPC is a specific induction mechanism of ETI and PCD. Upon NB-LRR activation, an unknown intracellular signal is generated and transduced to the NPC to promote the disruption of CPR5 oligomer. This NPC change coordinates CKIs release for ETI signaling and reconfigures the selective barrier to allow significant influx of nuclear signaling cargos through the NPC. These combined effects result in simultaneous activation of diverse stress-related nuclear signaling pathways that contribute to ETI/PCD.

See also Figure S6.

or undergoes any specific structural change to support these immune-activated transport events was previously unknown. Our study revealed that rather than a passive conduit, the NPC is both a signaling platform and a dynamic regulator of nucleocytoplasmic cargo transport. This dual function of the NPC is directed by CPR5 and plays a necessary and sufficient role for ETI/PCD induction.

CPR5 Is a Transmembrane Nucleoporin that Inhibits ETI by Modulating Selective Transport of the NPC

Multiple *cpr5* loss-of-function mutants have been reported to confer spontaneous cell death and NB-LRR-independent resistance to pathogens carrying virulence effectors (Boch et al., 1998; Bowling et al., 1997), yet a direct inhibitory role for CPR5 in ETI has only recently been demonstrated with overexpression of the wild-type CPR5 showing inhibition on effector-triggered PCD and resistance (Wang et al., 2014). Here, we demonstrate that CPR5 is a bona fide nucleoporin based on its NPC localization as well as physical and genetic interaction with the NPC core scaffold (Figures 1 and 2).

Cellular, genetic, and genomic analyses showed that CPR5 inhibits ETI/PCD by constraining nuclear accumulation of a diverse array of signaling cargos (Figures 3 and 4). The enhanced defense observed in *cpr5* is the opposite of the compromised basal and ETI resistance reported for the NPC scaffold nucleoporin mutants, which are defective in bulk mRNA export (Du et al., 2016; Wiermer et al., 2012; Zhang and Li, 2005). CPR5 appears to regulate nuclear transport of signaling cargos by affecting the selective barrier composed of FG proteins, because it is physically connected with the FG protein anchor Nup93 (Figure 2D–2F) and mutants of three individual FG proteins *Nup54*, *Nup58*, and *Nup136* each exacerbated the *cpr5* phenotype (Figure 4E). Importantly, mutating the FG proteins Nup54 and Nup136 alone led to enhancement of ETI, but not basal resistance (Figure 4F), suggesting that these FG proteins specifically inhibit ETI.

Disruption of CPR5 Homomeric Interaction Is an Induction Mechanism of ETI

CPR5 normally inhibits ETI at the NPC as a homomeric complex formed via its N-terminal extra-luminal domain (Figure 5). This inhibition is specifically "turned off" when CPR5 homomers are disrupted upon activation of an NB-LRR receptor RPS2 (Figures 6A–6C). Therefore, this conformational change of CPR5 in the NPC is a signaling event downstream of NB-LRRs. Moreover, this event appears to be sufficient for ETI/PCD activation as overexpression of either an N terminus-truncated CPR5 or the G120D mutant compromised in oligomer formation resulted in the *cpr5* phenotype in the WT background (Figures 6E and S3).

Disrupting the CPR5 oligomer significantly reduces its affinity to CKIs (Figure 6F), which provides a mechanistic explanation for our previous observation that CKIs are released from CPR5 for ETI induction (Wang et al., 2014). However, ectopic expression of CKIs alone is not sufficient for mounting ETI/PCD (Figure S6B), consistent with our genetic data indicating that NPC-gated cargo transport is also necessary. Therefore, disruption of CPR5 oligomerization coordinates the two NPC actions that are collaboratively required for ETI/PCD induction.

CPR5-Mediated CKI Release and NPC Permeabilization Is a Convergent Induction Mechanism by both CC-NB-LRR and TIR-NB-LRR

We propose that during ETI, in addition to activation of distinct receptors and their signaling complexes, a common signal is generated and transduced to the NPC, leading to a disruption of CPR5 oligomer. The resulting activation of the noncanonical CKI-Rb-E2F signaling module together with the influx of nuclear signaling cargos through the NPC leads to transcriptomic changes bearing signatures of diverse hormone and stress responses (Figures 3 and 4), which overlap significantly with those induced by both a CC-NB-LRR (RPS2) and a TIR-NB-LRR (RPS4) (Figure 6D). These CPR5-regulated and NPC-gated cellular responses were barely observed in basal immunity (Figure 6D), suggesting that ETI is more than a quantitative ramping-up of basal immunity even though the two defense mechanisms have some overlap in signaling networks (Tao et al., 2003; Tsuda et al., 2009). Our study suggests that the NPC contributes a specific regulatory mechanism for simultaneous activation of diverse stress responses, which ultimately lead to the extreme outcome of ETI, i.e., PCD.

It is tempting to compare the NB-LRR-triggered NPC alterations in plants to cellular changes associated with two distinct types of PCD in animals, apoptosis and pyroptosis. Activation of both types of PCD involves specialized mechanisms for membrane permeabilization to release pro-death factors. Activation of apoptosis requires formation of permeability transition pore (PTP) on mitochondrial membranes in order to release cytochrome *c* and other proteins for caspase-9 activation (Tait and Green, 2010), whereas activation of pyroptosis requires cleaved Gasdermin D to form pores on the plasma membrane to promote cell lysis and release of IL-1β (Ding et al., 2016). Our study showed that during ETI induction, the selective barrier of the NPC becomes more permeable through the conformational change of CPR5 to simultaneously activate diverse nuclear signaling events required for the activation of ETI and the execution of PCD in plants.

STAR★METHODS

Detailed methods are provided in the online version of this paper and include the following:

- KEY RESOURCES TABLE
- CONTACT FOR REAGENT AND RESOURCE SHARING
- EXPERIMENTAL MODEL AND SUBJECT DETAILS
  - Arabidopsis
- METHOD DETAILS
  - Plasmid Construction
  - Transient Expression Assays
  - Confocal Laser Scanning Microscopy
  - Immunoelectron Microscopy and Electron Tomography
  - Co-immunoprecipitation
  - LC-MS/MS and Data Analysis
  - qPCR
  - Microarray Procedure and Data Analysis

SUPPLEMENTAL INFORMATION

Supplemental Information includes six figures and three tables and can be found with this article online at http://dx.doi.org/10.1016/j.cell.2016.07.042.

AUTHOR CONTRIBUTIONS

Y.G., S.W., and X.D. designed the research. Y.G. performed most of the experiments. S.G.Z. contributed GEO: GSE72742. Z.L. and B.-H.K. performed the immunoelectron microscopy. S.W. helped with the protein complex purification. Y.G. and X.D. wrote the paper with comments from all authors.

ACKNOWLEDGMENTS

The authors thank Dr. Roger Innes for providing membrane organelle markers and Dr. Iris Meier for sharing the *35S:GFP-WIP1* and *35S:RanGAP1-GFP* transgenic lines. We also thank Drs. Iris Meier, Paul Zwack, and John Withers for critical reading of the manuscript. This work was supported by the Howard Hughes Medical Institute and the Gordon and Betty Moore Foundation (through grant GBMF3032) and grants from the NIH (R01-GM069594 to X.D.), the National Natural Science Foundation of China (grant 31571254 to S.W.), the Rural Development Administration, Republic of Korea (project 10953092015), and the Research Grants Council of Hong Kong (AoE/M-05/12, C4011-14R to B.K.).

Received: January 29, 2016
Revised: June 15, 2016
Accepted: July 26, 2016
Published: August 25, 2016

REFERENCES

Alber, F., Dokudovskaya, S., Veenhoff, L.M., Zhang, W., Kipper, J., Devos, D., Suprapto, A., Karni-Schmidt, O., Williams, R., Chait, B.T., et al. (2007). The molecular architecture of the nuclear pore complex. Nature *450*, 695–701.

Anderson, L.K. (2006). CPR5 encodes a novel protein required for endoreduplication and cell expansion in plants. PhD thesis (Duke University).

Boch, J., Verbsky, M.L., Robertson, T.L., Larkin, J.C., and Kunkel, B.N. (1998). Analysis of resistance gene-mediated defense responses in Arabidopsis thaliana plants carrying a mutation in CPR5. Mol. Plant Microbe Interact. *11*, 1196–1206.

Bowling, S.A., Clarke, J.D., Liu, Y., Klessig, D.F., and Dong, X. (1997). The cpr5 mutant of Arabidopsis expresses both NPR1-dependent and NPR1-independent resistance. Plant Cell *9*, 1573–1584.

Brkljacic, J., Zhao, Q., and Meier, I. (2009). WPP-domain proteins mimic the activity of the HSC70-1 chaperone in preventing mistargeting of RanGAP1-anchoring protein WIT1. Plant Physiol. *151*, 142–154.

Chakraborty, P., Wang, Y., Wei, J.H., van Deursen, J., Yu, H., Malureanu, L., Dasso, M., Forbes, D.J., Levy, D.E., Seemann, J., and Fontoura, B.M. (2008). Nucleoporin levels regulate cell cycle progression and phase-specific gene expression. Dev. Cell *15*, 657–667.

Cheng, Y.T., Germain, H., Wiermer, M., Bi, D., Xu, F., García, A.V., Wirthmueller, L., Després, C., Parker, J.E., Zhang, Y., and Li, X. (2009). Nuclear pore complex component MOS7/Nup88 is required for innate immunity and nuclear accumulation of defense regulators in Arabidopsis. Plant Cell *21*, 2503–2516.

Chug, H., Trakhanov, S., Hülsmann, B.B., Pleiner, T., and Görlich, D. (2015). Crystal structure of the metazoan Nup62●Nup58●Nup54 nucleoporin complex. Science *350*, 106–110.

Deslandes, L., and Rivas, S. (2011). The plant cell nucleus: a true arena for the fight between plants and pathogens. Plant Signal. Behav. *6*, 42–48.

Ding, J., Wang, K., Liu, W., She, Y., Sun, Q., Shi, J., Sun, H., Wang, D.C., and Shao, F. (2016). Pore-forming activity and structural autoinhibition of the gasdermin family. Nature *535*, 111–116.

Dong, C.H., Hu, X., Tang, W., Zheng, X., Kim, Y.S., Lee, B.H., and Zhu, J.K. (2006). A putative Arabidopsis nucleoporin, AtNUP160, is critical for RNA export and required for plant tolerance to cold stress. Mol. Cell. Biol. *26*, 9533–9543.

Du, J., Gao, Y., Zhan, Y., Zhang, S., Wu, Y., Xiao, Y., Zou, B., He, K., Gou, X., Li, G., et al. (2016). Nucleocytoplasmic trafficking is essential for BAK1- and BKK1-mediated cell-death control. Plant J. *85*, 520–531.

Elmore, J.M., Lin, Z.J., and Coaker, G. (2011). Plant NB-LRR signaling: upstreams and downstreams. Curr. Opin. Plant Biol. *14*, 365–371.

García, A.V., and Parker, J.E. (2009). Heaven's Gate: nuclear accessibility and activities of plant immune regulators. Trends Plant Sci. *14*, 479–487.

Geisler-Lee, J., O'Toole, N., Ammar, R., Provart, N.J., Millar, A.H., and Geisler, M. (2007). A predicted interactome for Arabidopsis. Plant Physiol. *145*, 317–329.

Gilmore, T.D. (2006). Introduction to NF-kappaB: players, pathways, perspectives. Oncogene *25*, 6680–6684.

Gong, F.C., Giddings, T.H., Meehl, J.B., Staehelin, L.A., and Galbraith, D.W. (1996). Z-membranes: artificial organelles for overexpressing recombinant integral membrane proteins. Proc. Natl. Acad. Sci. USA *93*, 2219–2223.

Gu, Y., and Innes, R.W. (2011). The KEEP ON GOING protein of Arabidopsis recruits the ENHANCED DISEASE RESISTANCE1 protein to trans-Golgi network/early endosome vesicles. Plant Physiol. *155*, 1827–1838.

Gu, Y., and Innes, R.W. (2012). The KEEP ON GOING protein of Arabidopsis regulates intracellular protein trafficking and is degraded during fungal infection. Plant Cell *24*, 4717–4730.

Jevtić, P., Edens, L.J., Vuković, L.D., and Levy, D.L. (2014). Sizing and shaping the nucleus: mechanisms and significance. Curr. Opin. Cell Biol. *28*, 16–27.

Jing, H.C., Anderson, L., Sturre, M.J., Hille, J., and Dijkwel, P.P. (2007). Arabidopsis CPR5 is a senescence-regulatory gene with pleiotropic functions as predicted by the evolutionary theory of senescence. J. Exp. Bot. *58*, 3885–3894.

Jones, J.D., and Dangl, J.L. (2006). The plant immune system. Nature *444*, 323–329.

Kang, B.H. (2010). Electron microscopy and high-pressure freezing of Arabidopsis. Methods Cell Biol. *96*, 259–283.

Lee, H., Xiong, L., Gong, Z., Ishitani, M., Stevenson, B., and Zhu, J.K. (2001). The Arabidopsis HOS1 gene negatively regulates cold signal transduction and encodes a RING finger protein that displays cold-regulated nucleo–cytoplasmic partitioning. Genes Dev. *15*, 912–924.

Lee, Y., Lee, H.S., Lee, J.S., Kim, S.K., and Kim, S.H. (2008). Hormone- and light-regulated nucleocytoplasmic transport in plants: current status. J. Exp. Bot. *59*, 3229–3245.

Mans, B.J., Anantharaman, V., Aravind, L., and Koonin, E.V. (2004). Comparative genomics, evolution and origins of the nuclear envelope and nuclear pore complex. Cell Cycle *3*, 1612–1637.

McNellis, T.W., Mudgett, M.B., Li, K., Aoyama, T., Horvath, D., Chua, N.H., and Staskawicz, B.J. (1998). Glucocorticoid-inducible expression of a bacterial avirulence gene in transgenic Arabidopsis induces hypersensitive cell death. Plant J. *14*, 247–257.

Nelson, B.K., Cai, X., and Nebenführ, A. (2007). A multicolored set of in vivo organelle markers for co-localization studies in Arabidopsis and other plants. Plant J. *51*, 1126–1136.

O'Connor, T.R., Dyreson, C., and Wyrick, J.J. (2005). Athena: a resource for rapid visualization and systematic analysis of Arabidopsis promoter sequences. Bioinformatics *21*, 4411–4413.

Palma, K., Zhang, Y., and Li, X. (2005). An importin alpha homolog, MOS6, plays an important role in plant innate immunity. Curr. Biol. *15*, 1129–1135.

Parry, G. (2014). Components of the Arabidopsis nuclear pore complex play multiple diverse roles in control of plant growth. J. Exp. Bot. *65*, 6057–6067.

Parry, G., Ward, S., Cernac, A., Dharmasiri, S., and Estelle, M. (2006). The Arabidopsis SUPPRESSOR OF AUXIN RESISTANCE proteins are nucleoporins with an important role in hormone signaling and development. Plant Cell *18*, 1590–1603.

Reina-Pinto, J.J., Voisin, D., Teodor, R., and Yephremov, A. (2010). Probing differentially expressed genes against a microarray database for in silico suppressor/enhancer and inhibitor/activator screens. Plant J. *61*, 166–175.

Rivas, S. (2012). Nuclear dynamics during plant innate immunity. Plant Physiol. *158*, 87–94.

Shulga, N., Mosammaparast, N., Wozniak, R., and Goldfarb, D.S. (2000). Yeast nucleoporins involved in passive nuclear envelope permeability. J. Cell Biol. *149*, 1027–1038.

Strambio-De-Castillia, C., Niepel, M., and Rout, M.P. (2010). The nuclear pore complex: bridging nuclear transport and gene regulation. Nat. Rev. Mol. Cell Biol. *11*, 490–501.

Stuart, L.M., Paquette, N., and Boyer, L. (2013). Effector-triggered versus pattern-triggered immunity: how animals sense pathogens. Nat. Rev. Immunol. *13*, 199–206.

Tait, S.W., and Green, D.R. (2010). Mitochondria and cell death: outer membrane permeabilization and beyond. Nat. Rev. Mol. Cell Biol. *11*, 621–632.

Tamura, K., Fukao, Y., Iwamoto, M., Haraguchi, T., and Hara-Nishimura, I. (2010). Identification and characterization of nuclear pore complex components in Arabidopsis thaliana. Plant Cell *22*, 4084–4097.

Tao, Y., Xie, Z., Chen, W., Glazebrook, J., Chang, H.S., Han, B., Zhu, T., Zou, G., and Katagiri, F. (2003). Quantitative nature of Arabidopsis responses during compatible and incompatible interactions with the bacterial pathogen Pseudomonas syringae. Plant Cell *15*, 317–330.

Toyama, B.H., Savas, J.N., Park, S.K., Harris, M.S., Ingolia, N.T., Yates, J.R., 3rd, and Hetzer, M.W. (2013). Identification of long-lived proteins reveals exceptional stability of essential cellular structures. Cell *154*, 971–982.

Tsuda, K., Sato, M., Stoddard, T., Glazebrook, J., and Katagiri, F. (2009). Network properties of robust immunity in plants. PLoS Genet. *5*, e1000772.

Verslues, P.E., Guo, Y., Dong, C.H., Ma, W., and Zhu, J.K. (2006). Mutation of SAD2, an importin beta-domain protein in Arabidopsis, alters abscisic acid sensitivity. Plant J. *47*, 776–787.

Wang, S., Gu, Y., Zebell, S.G., Anderson, L.K., Wang, W., Mohan, R., and Dong, X. (2014). A noncanonical role for the CKI-RB-E2F cell-cycle signaling pathway in plant effector-triggered immunity. Cell Host Microbe *16*, 787–794.

Washburn, M.P., Wolters, D., and Yates, J.R., 3rd. (2001). Large-scale analysis of the yeast proteome by multidimensional protein identification technology. Nat. Biotechnol. *19*, 242–247.

Wiermer, M., Cheng, Y.T., Imkampe, J., Li, M., Wang, D., Lipka, V., and Li, X. (2012). Putative members of the Arabidopsis Nup107-160 nuclear pore subcomplex contribute to pathogen defense. Plant J. *70*, 796–808.

Wirthmueller, L., Roth, C., Banfield, M.J., and Wiermer, M. (2013). Hop-on hop-off: importin-α-guided tours to the nucleus in innate immune signaling. Front. Plant Sci. *4*, 149.

Yi, X., Du, Z., and Su, Z. (2013). PlantGSEA: a gene set enrichment analysis toolkit for plant community. Nucleic Acids Res. *41*, W98–W103.

Yoshida, S., Ito, M., Nishida, I., and Watanabe, A. (2002). Identification of a novel gene HYS1/CPR5 that has a repressive role in the induction of leaf senescence and pathogen-defence responses in Arabidopsis thaliana. Plant J. *29*, 427–437.

Zhang, Y., and Li, X. (2005). A putative nucleoporin 96 Is required for both basal defense and constitutive resistance responses mediated by suppressor of npr1-1,constitutive 1. Plant Cell *17*, 1306–1316.

STAR★METHODS

KEY RESOURCES TABLE

REAGENT or RESOURCE	SOURCE	IDENTIFIER
Antibodies		
Mouse monoclonal anti-GFP (JL-8, for western blot)	Clontech	Cat. #632381; RRID: AB_2313808
Rabbit polyclonal anti-GFP (for immuno-EM)	Santa Cruz	Cat. #sc-8334; RRID: AB_641123
Mouse monoclonal anti-HA (16B12)	Biolegend	Cat. #901502; RRID: AB_2565007
Alpaca anti-GFP coupled to agarose beads	Chromotek	Cat. #GFP-Trap_A
Pierce Anti-HA Agarose	Thermofisher	Cat. #26181; RRID: AB_2537081
Chemicals, Peptides, and Recombinant Proteins		
Dexamethasone	Sigma-Aldrich	Cat. #D1756-25MG; CAS: 50-02-2
DAPI	Sigma-Aldrich	Cat. #D9542-5MG; CAS: 28718-90-3
LR Clonase II Plus enzyme	Thermofisher	Cat. #12538120
Protease inhibitor cocktail	Sigma-Aldrich	Cat. #P9599-5ML; EC: 200-664-3
TRIzol Reagent	Thermofisher	Cat. #15596026
Critical Commercial Assays		
QuikChange II site-directed mutagenesis kit	Agilent	Cat. #200524
Wheat germ in vitro translation system	BioSieg	N/A
SuperScript III First-Strand Synthesis System	Thermofisher	Cat. #18080050
FastStart Universal SYBR Green Master Kit	Roche	Cat. # 04913850001
Deposited Data		
Microarray raw and analyzed data	This paper	GEO: GSE72742, GSE72743
Experimental Models: Organisms/Strains		
Arabidopsis: 35S::GFP-CPR5	Wang et al., 2014	N/A
Arabidopsis: 35S::YFP-CPR5/G120D	This paper	N/A
Arabidopsis: 35S/Dex::YFP-CPR5-C	This paper	N/A
Arabidopsis: 35S::(nYFP-CPR5+cYFP-CPR5)	This paper	N/A
Arabidopsis: 35S::(GFP-CPR5+3HA-CPR5)	This paper	N/A
Arabidopsis: GFP-WIP1	The Meier Laboratory	N/A
Arabidopsis: Nup155-YFP	This paper	N/A
Arabidopsis: MOS7-GFP	Cheng et al., 2009	N/A
nup88 (*mos7-1*), *nup96* (*mos3-1*), *importin-α3* (*mos6-2*)	The Li Laboratory, Cheng et al., 2009; Zhang and Li, 2005; Palma et al., 2005	N/A
All other nucleoporin and transport receptor mutants used in this study, see Table S2	*Arabidopsis* Biological Resource Center	see Table S2 for Salk line ID
Arabidopsis: 35S::YFP-SIM	This paper	N/A
Arabidopsis: Dex::AvrRpt2	McNellis et al., 1998	N/A
Recombinant DNA		
pMDC43-GFP-CPR5	Wang et al., 2014	N/A
pEG100-YFP-CPR5 (WT and mutant constructs)	This paper	N/A
pEG100-n/cYFP-CPR5	This paper	N/A
pEG100-Nups-YFP/cYFP	This paper	N/A
pBAV154/pEG100-YFP-CPR5-C	This paper	N/A
pEG100-NPR1/JAZ1/ABI5-mCherry	This paper	N/A
pEG100-mCherry-WIT1	This paper	N/A

(*Continued on next page*)

Continued

REAGENT or RESOURCE	SOURCE	IDENTIFIER
Sequence-Based Reagents		
Primers used in this study, see Table S3	This paper	N/A
Software and Algorithms		
Mascot (v2.5.0)	Matrix Science	N/A
Scaffold (v4.4.1.1)	Proteome Software	N/A
R (v3.0.1)	N/A	N/A
GeneSpring (v13.0)	Agilent	N/A
MASTA	Reina-Pinto et al., 2010	N/A
PlantGSEA	Yi et al., 2013	http://structuralbiology.cau.edu.cn/PlantGSEA/
Athena	O'Connor et al., 2005	

CONTACT FOR REAGENT AND RESOURCE SHARING

Further information and requests for reagents may be directed to, and will be fulfilled by the corresponding author Xinnian Dong (xdong@duke.edu).

EXPERIMENTAL MODEL AND SUBJECT DETAILS

Arabidopsis

All *Arabidopsis* plants used in this study were in the Col-0 background. Wild-type (WT), mutant, and transgenic *Arabidopsis* seeds were stratified at 4°C for two days and plants were grown under a 12 hr light and 12 hr dark cycle at 22°C. *GFP-WIP1, NPR1-GFP, Nup155-YFP* and *MOS7-GFP* were introduced into the *cpr5* mutant background through genetic crosses. Nucleoporin and transport receptor mutants used in this study were Salk T-DNA insertion lines obtained from *Arabidopsis* Biological Resource Center (see Table S2 for Salk line information) or *mos* mutants (Cheng et al., 2009; Palma et al., 2005; Zhang and Li, 2005) provided by Dr. Xin Li's laboratory (see Table S2). *cpr5 nup* double mutants were obtained through genetic crosses. *35S:YFP-CPR5-C* and *Dex:YFP-CPR5-C* were transformed into WT background for functional interference of CPR5 and subsequently crossed to the *cpr5* mutant as controls to test the specificity of the interference effect. To obtain *35S:GFP-CPR5/HA-CPR5* double transgenic line, a previously reported *35S:GFP-CPR5* line (Wang et al., 2014) was transformed with *35S:HA-CPR5*. T3 progeny homozygous for both transgenes were used for experiments. Isogenic *35S:n/cYFP-CPR5* line and *Dex:AvrRpt2* line (McNellis et al., 1998) were generated in WT and *rps2* backgrounds, respectively. The *35S:n/cYFP-CPR5 /Dex:AvrRpt2* double transgenic lines were obtained by genetic crosses.

METHOD DETAILS

Plasmid Construction

All point mutations of *CPR5* were generated using the QuikChange II site-directed mutagenesis kit (Agilent). The full-length cDNA of *CPR5*, *WIT1*, *SIM* and all *CPR5* mutant constructs including the single-site mutations and truncations were cloned into pBSDONR p4r-p2, a multisite gateway donor vector for N-terminal tagging (Gu and Innes, 2011). The full-length cDNA of *Nup136*, *Nup93a*, *Nup35*, *NPR1*, *JAZ1*, *ABI5* and the genomic DNA fragments (from start codon to stop codon) of *Nup155*, *Nup96*, *Nup88*, *Nup85*, *Nup62*, *Nup58*, *Nup54*, *HOS1* were cloned into pBSDONR p1-p4, a multisite gateway donor vector for C-terminal tagging. Those clones were then paired with fluorescent tags, n/c-YFP (for BiFC) or 3xHA tag cloned in pBSDONR p1-p4 or pBSDONR p4r-p2, to generate fusion constructs in pEG100 or pBAV154 destination vector by LR reaction (LR clonase II plus, Thermofisher) for constitutive or dexamethasone inducible expression, respectively. To generate *35S:n/cYFP-CPR5* construct used in transgenic line, *nYFP-CPR5* was first cloned in pGWB414 by LR reaction and a fragment including the promoter, the fusion construct and the terminator was amplified, cut by AseI and ligated into pEG100, which already contains an independent expression cassette for the *cYFP-CPR5* fusion. All constructs were verified by sequencing before use.

Transient Expression Assays

Agrobacterium-mediated transient expression in *N. benthamiana* and transformation of *Arabidopsis* protoplasts were performed as described (Gu and Innes, 2011).

Confocal Laser Scanning Microscopy

Intracellular fluorescence was observed using a Leica SP8 upright confocal microscope with high sensitivity hybrid detectors. Intracellular membrane organelle markers used were described previously (Brkljacic et al., 2009; Gu and Innes, 2011, 2012; Nelson et al., 2007). Three-dimensional image reconstruction and co-localization statistics were carried out using IMARIS 8.0 (Bitplane). FRAP experiment was performed using Leica SP8 FRAP Wizard. Fluorescence intensity was normalized to the average expression level defined by random sampling before photobleaching. Recovery curves were plotted with 50 frames (1 frame/sec) recorded after photobleaching.

Immunoelectron Microscopy and Electron Tomography

Root tip samples were dissected from *Arabidopsis* seedlings expressing GFP-CPR5 and cryofixed by an HPM100 (Leica Microsystems). The frozen specimens were freeze-substituted at −80°C and embedded in HM20 resin (Electron Microscopy Sciences) at −45°C. After polymerization at −45°C, the root tip samples were sectioned and immunolabeled with a GFP antibody (Santa Cruz) as described previously (Kang, 2010).

Co-immunoprecipitation

All tagged proteins for in vitro pull-down assays were synthesized using a wheat germ-based translation system (BioSieg). Synthesized proteins were mixed and incubated with GFP-TrapA (Chromo Tek) or Pierce anti-HA agarose beads (Thermofisher) overnight at 4°C in the pull-down buffer (50 mM Tris [pH 7.5], 150 mM NaCl, 0.1% Triton X-100, 0.2% Nonidet P-40, plant protease inhibitor cocktail (Sigma) and 40 μM MG115). Following immunoprecipitation (IP), beads were precipitated and washed five times with the pull-down buffer before eluted with the SDS sample buffer. For in vivo co-immunoprecipitation, leaf tissues of four-week-old transgenic plants were collected. Total protein was extracted using IP buffer with high concentration of detergents to completely solubilize membrane protein (50 mM Tris [pH 7.5], 150 mM NaCl, 0.5% Triton X-100, 0.5% Nonidet P-40, 0.25% Na-deoxycholate, plant protease inhibitor cocktail, and 40 mM MG115) followed by immunoprecipitation with GFP-TrapA beads overnight at 4°C. After IP, beads were washed five times with the IP buffer. Samples were boiled with loading buffer for 10 min before separated by SDS-PAGE.

LC-MS/MS and Data Analysis

A total of 5 g leaf tissues from four-week-old transgenic plants were collected. Total protein was extracted with IP buffer (50 mM Tris [pH 7.5], 150 mM NaCl, 0.5% Triton X-100, 0.5% Nonidet P-40, 0.25% Nadeoxycholate, plant protease inhibitor cocktail, and 40 mM MG115) and immunoprecipitated with GFP-TrapA beads overnight at 4°C. After IP, samples were washed five times with the IP buffer and three times with 50 mM NH_4HCO_3 before on-bead trypsin digestion. Following immunoprecipitation, on-bead trypsin digestion, peptide lyophilization and LC-MS/MS were performed by the Duke Proteomics Core Facility. MS/MS samples were analyzed using Mascot (Matrix Science, London, UK; version 2.5.0) and searched with a fragment ion mass tolerance of 0.020 Da and a parent ion tolerance of 5.0 PPM. Scaffold (version 4.4.1.1, Proteome Software, Portland, OR) was used to validate MS/MS based peptide and protein identifications. Peptide/protein identifications were accepted if they could be established at greater than 95% probability by the Peptide/Protein Prophet algorithm, which yielded a false-discovery rate of 0.1% and 0.5% on the peptide and protein match level, respectively. Data from *35S:GFP* samples ran in parallel were used as controls for a statistical model-based selection of CPR5-specific interactors. The resulting list was shortened to 28 by further excluding proteins that are abundant in chloroplasts and mitochondria. Predicted interactions between CPR5 interactors were based on an interolog method (Geisler-Lee et al., 2007).

qPCR

Arabidopsis RNA was extracted using TRIzol Reagent (Thermofisher), and cDNA was synthesized using the SuperScript III cDNA Synthesis (Thermofisher). qPCR was performed using FastStart Universal SYBR Green Master Kit (Roche) in Mastercycler ep realplex (Eppendorf).

Microarray Procedure and Data Analysis

For *RPS2*-dependent ETI response, four-week-old WT and *rps2* mutant plants were inoculated with *Psm/AvrRpt2*. At 0, 6 and 10 hr post inoculation, leaf tissues were collected for RNA preparation and microarray. The resulting dataset was deposited to GEO: GSE72742. For transient interference of the CPR5 function, four-week-old WT and T3 homozygous *Dex:YFP-CPR5-C* transgenic plants were sprayed with water or 50 μM dexamethasone (Sigma). After 24 hr, leaf tissues were collected for RNA preparation and microarray. The resulting dataset was deposited to GEO: GSE72743. RNA quality control, cDNA synthesis, aRNA purification and fragmentation, hybridization, washing, and scanning of *Arabidopsis* ATH1 Genome Arrays (Affymetrix) chips were performed by the Duke Microarray Facility. For CPR5-C interference microarray, differentially expressed genes were further filtered by subtracting genes whose expression are affected by the empty vector control upon dexamethasone induction (GEO: GSE8741). The resulting gene list was provided in Table S1. The *RPS4*-dependent ETI genes, *RPS2*-dependent ETI genes and basal immunity genes were determined by microarray analysis of dataset GEO: GSE50019, GSE73742 and GSE17464, respectively. Statistical analysis and natural language processing-based network regulator discovery were performed using GeneSpring 13.0 (Agilent, 2014) and R 3.0.1

(2013). Networks were established based on published transcriptional regulatory relationships between genes and physical interactions between proteins. Comparative microarray analysis and GSEA were performed using MASTA (Reina-Pinto et al., 2010) and PlantGSEA (Yi et al., 2013), respectively. *Cis*-element enrichment was analyzed using total differentially expressed genes with Athena (O'Connor et al., 2005).

Bacterial Growth Assay

Infection of *Arabidopsis* plants with *Psm* ES4326 (with or without *AvrRpt2*) was performed as described previously (Wang et al., 2014). Bacterial suspension of OD_{600nm} = 0.001 was infiltrated into 2 leaves per plant and 12 plants per genotype. Each experimental replication contained four leaf discs from two plants. Bacterial growth was quantified at 0 and 3 days post infiltration.

Primers

All primers used in this study were listed in Table S3.

QUANTIFICATION AND STATISTICAL ANALYSIS

The nuclear circularity index is defined as $4\pi A/P^2$, where A and P are the cross-sectional area and perimeter of the nucleus, respectively. A and P were measured for each nucleus using Fiji. Bacterial growth was reported as the number of colony forming units (cfu), which was subject to log transformation. For fluorescence quantification using Fiji, the fluorescence intensity was calculated using Integrated Density – (Area of selected cell × Mean fluorescence of background). Nuclear circularity, log(cfu) and fluorescence intensity data were assumed to follow normal distributions and were subjected to two-tailed Student's t test or ANOVA, where appropriate. Statistical tests were performed in GraphPad Prism 6. Statistical parameters including the exact value of n, the definition of center, dispersion, and precision measures (mean ± SDM) and statistical significance can be found in the Figure Legends. In Figures, asterisks denote statistical significance test (*, $p < 0.05$; **, $p < 0.01$; ***, $p < 0.001$; ****, $p < 0.0001$) as compared to untreated controls, unless otherwise specified by lines connecting the compared pieces of data. For LC-MS/MS analysis, exclusive spectrum count data were assumed to follow a Gamma-Poisson distribution. After normalized by size factors, negative binomial regression models were built with the normalized data using DESeq2 package in R, which provided the cutoff to select for CPR5-specific interactors (p value < 0.05, fold change > 2.5, CPR5 versus GFP). For microarray analysis, array data were summarized using the Robust Multiarray Average method using GeneSpring and the normal distribution of the expression data were verified using EMA package in R. CPR5-C-induced differentially expressed genes were selected using 2-way ANOVA model (p value < 0.01, fold change > 2, dex versus water); the *RPS4*-dependent ETI genes were determined by 2-way ANOVA (p value < 0.01, fold change > 2) using the signaling mutant *eds1* as a control (GEO: GSE50019); the *RPS2*-dependent ETI genes induced by *Psm/AvrRpt2* was determined by 2-way ANOVA (p value < 0.01, fold change > 2) using the immune receptor mutant *rps2* as a control (GEO: GSE72742); the basal immunity induced by *Pst* DC3000 was determined by Moderated t test (p value < 0.05 and fold change > 2, GEO: GSE17464).

DATA AND SOFTWARE AVAILABILITY

Data Resources

Raw data files for the microarray analysis have been deposited in the NCBI GEO under accession numbers GEO: GSE72742 and GSE72743.

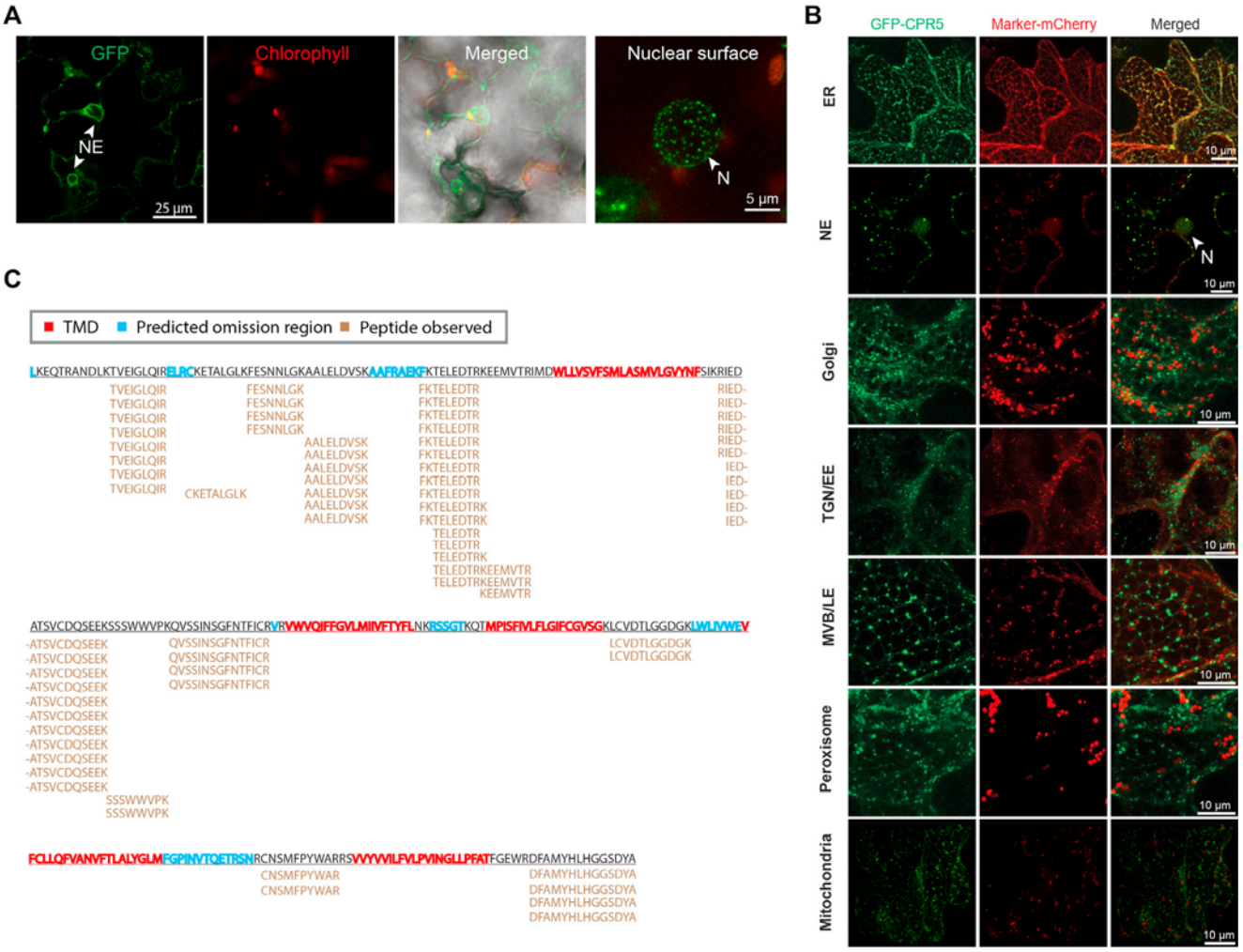

Figure S1. CPR5 Is a Transmembrane Protein Enriched in the Nuclear Pore, Related to Figure 1

(A) Leaf epidermal cells of two-week-old *35S:GFP-CPR5/cpr5-1* transgenic *Arabidopsis* seedlings were imaged using confocal laser scanning microscopy. Three-dimensional image of the nuclear surface was reconstructed from z stack images using Imaris (right). Arrowheads indicate the nuclear envelope (NE) or the nucleus (N).

(B) Co-localization of GFP-CPR5 with endomembrane markers. GFP-CPR5 was transiently co-expressed with mCherry-tagged endomembrane markers in *N. benthamiana*. The nuclear envelope (NE) marker is mCherry-WIT1. TGN/EE, *trans*-Golgi network/early endosome. MVB/LE, multi-vesicular body/late endosome.

(C) Peptide coverage of the carboxyl terminal half of the AtCPR5 protein. GFP-CPR5 was affinity purified from transgenic plants and subject to LC-MS/MS. The predicted transmembrane domains in CPR5 are labeled in red. Predicted omission regions by trypsin digestion are labeled in cyan. Individual peptides detected by LC-MS/MS are labeled in brown and listed below the reference sequence.

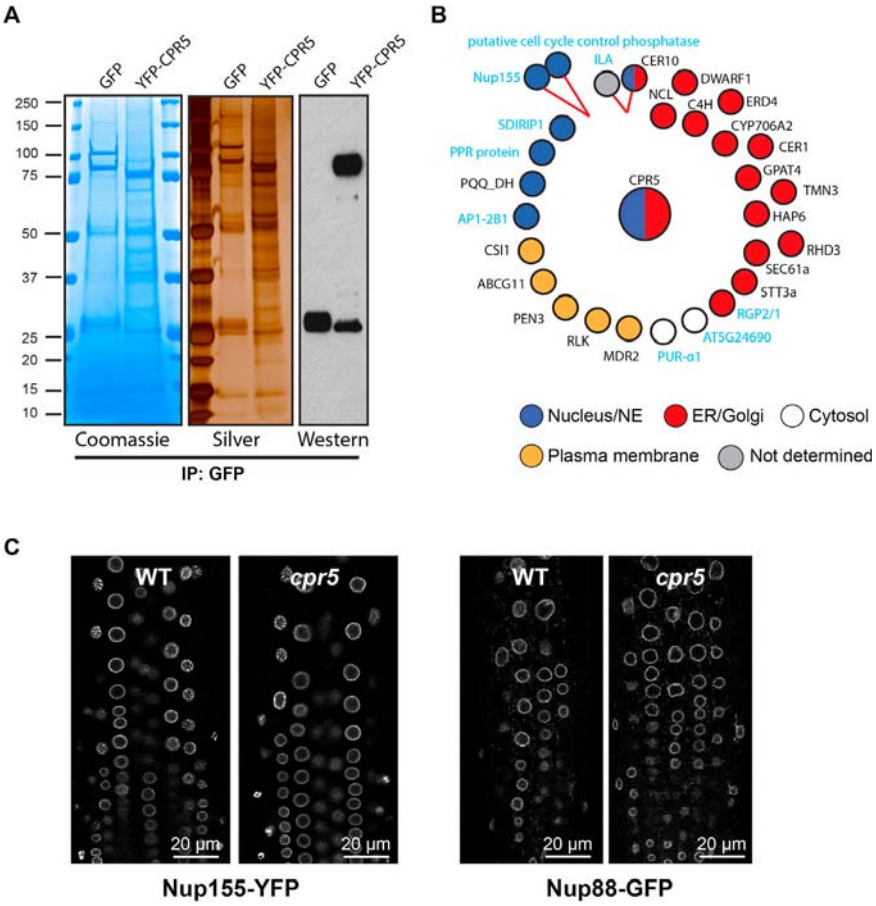

Figure S2. Identification of CPR5 Interactors and Localization of Nucleoporins in the *cpr5* Mutant, Related to Figure 2

(A) CPR5 protein complex purification. Total protein extracts from four-week-old *35S:YFP-CPR5* and *35S:GFP* transgenic plants were subject to immunoprecipitation using GFP-TrapA agarose beads. Before LC-MS/MS, sample aliquots were loaded onto SDS-PAGE and stained with Coomassie Blue, silver nitrate or blotted with the GFP antibody.

(B) The complete list of CPR5-specific interactors identified by protein complex purification. Subcellular localization of the proteins was color coded and determined by published fluorescent imaging studies or by transient expression of YFP-tagged protein in this study. Proteins with or without putative transmembrane domains are labeled with black and cyan in text, respectively. Interactions between CPR5 interactors (attached circles) were predicted by the interolog method (Geisler-Lee et al., 2007), indicating identification of putative protein complexes.

(C) Localization of Nup155 and Nup88 in WT and the *cpr5* mutant backgrounds. Isogenic *35S:Nup155-YFP* and *35S:Nup88-GFP* lines were generated in WT and *cpr5-1* backgrounds. Root cells of five-day-old seedlings were imaged.

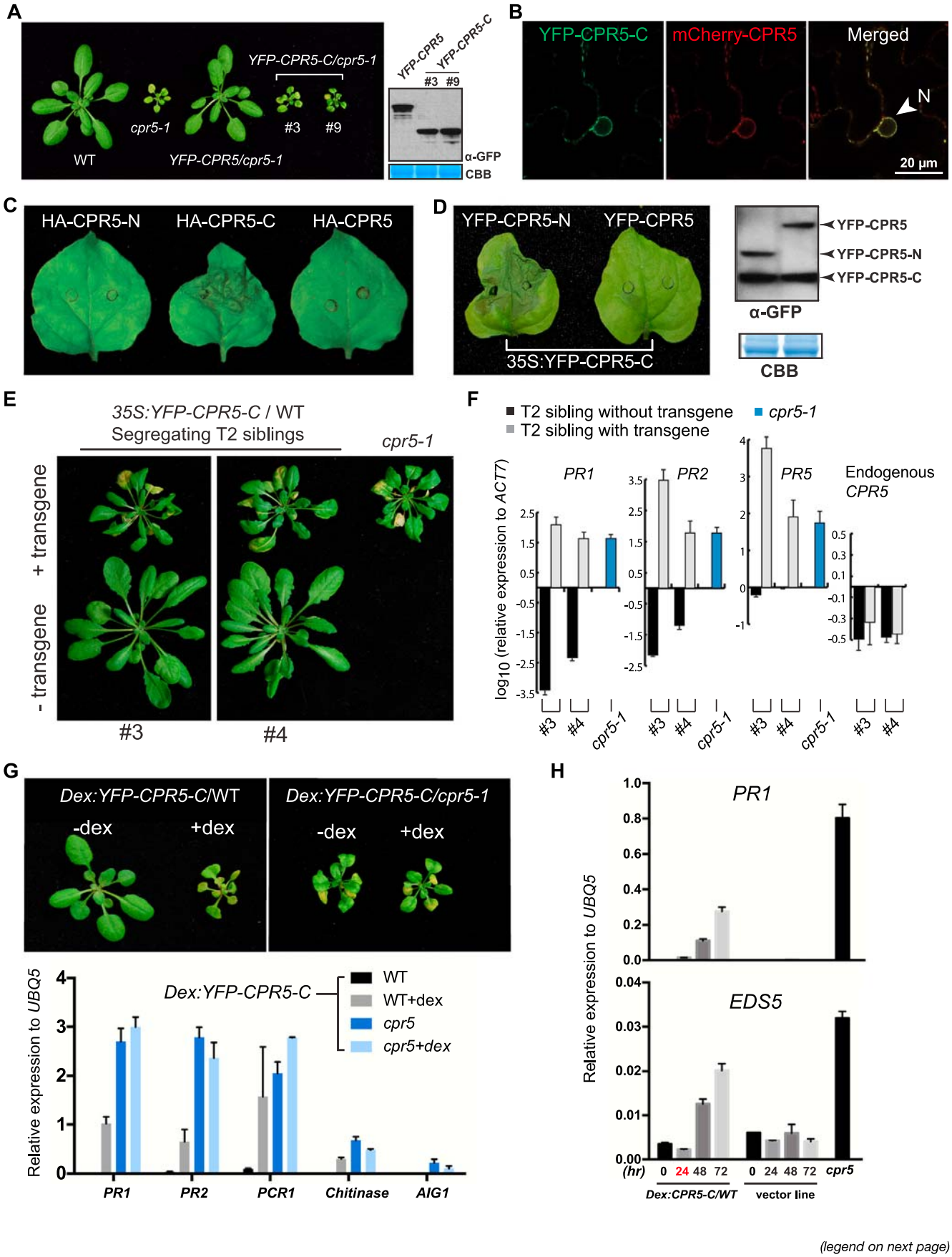

(legend on next page)

Figure S3. Overexpression of CPR5-C Interferes with the Function of the Endogenous CPR5 Protein, Related to Figure 3

(A) CPR5-C did not complement the *cpr5* mutant phenotypes. Two independent transgenic lines are shown. WT, the *cpr5* mutant and the complemented line expressing the full-length CPR5 are shown as control. Expression levels of transgenes are shown in the right panel.

(B) CPR5-C co-localizes with CPR5. YFP-CPR5-C and mCherry-CPR5 were transiently co-expressed in *N. benthamiana* and epidermal cells were imaged 24 hr after *Agrobacterium* infiltration. The arrowhead indicates the nucleus (N).

(C and D) Transient expression of HA-CPR5-C but not HA-CPR5-N or HA-CPR5 induced PCD in *N. benthamiana* (C). PCD induced by transient expression of YFP-CPR5-C could be suppressed by coexpression of YFP-CPR5 but not YFP-CPR5-N (D, left) at comparable protein levels (D, right). All constructs are driven by the 35S promoter. Representative leaves were photographed at 36 hr after *Agrobacterium* infiltration.

(E) Segregating T2 progeny of *35S:YFP-CPR5-C* transgenic *Arabidopsis* lines in WT background. The presence of the transgene was determined by PCR. Two independent lines (#3 and #4) are shown and *cpr5-1* mutant served as a control.

(F) qRT-PCR analysis of SA-dependent defense gene expression in *35S:YFP-CPR5-C* transgenic lines. The transcript levels of the endogenous CPR5 were not affected in the *35S:YFP-CPR5-C* lines (right). Data are presented as mean ± SDM (n = 3 biological replicates).

(G) Inducible expression of CPR5-C is innocuous in the *cpr5* mutant. Isogenic *Dex:YFP-CPR5-C* lines in WT and the *cpr5* mutant background were imaged 5 days after dexamethasone treatment (upper panel). Relative expression levels of most induced defense genes in the *cpr5* mutant were measured 3 days after dexamethasone treatment using qRT-PCR (lower panel). Data are presented as mean ± SDM (n = 2 biological replicates).

(H) Time course qRT-PCR analysis of SA-responsive genes in *Dex:YFP-CPR5-C* transgenic plants (WT background) after dexamethasone application. Relative expression levels of SA responsive (*PR1*) and transport (*EDS5*) genes were measured. A transgenic line with the empty vector and the *cpr5* mutant served as controls. Data are presented as mean ± SDM (n = 2 technical replicates). Similar results were obtained in two independent experiments.

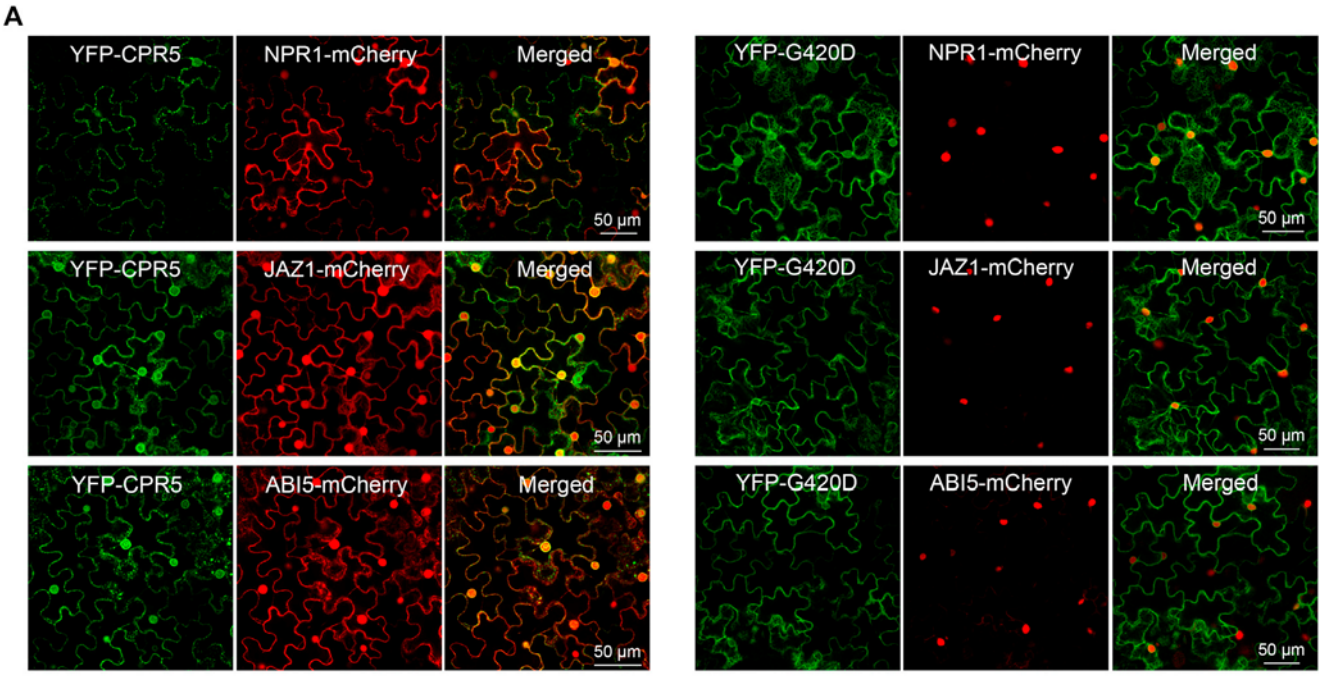

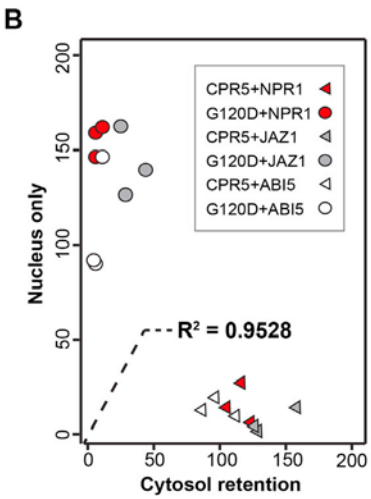

C

Cross	Karyopherin or Nup function	Phenotype
cpr5 mos6	importin α3	*cpr5*
cpr5 sad2	importin β2	*cpr5*
cpr5 nup88	cytoplasmic linker Nup	suppresion of *cpr5* dwarfism & PCD
cpr5 nup54	central channel FG Nup	enhancement of *cpr5* dwarfism
cpr5 nup58	central channel FG Nup	enhancement of *cpr5* dwarfism
cpr5 nup136	nuclear basket FG Nup	enhancement of *cpr5* dwarfism & PCD, partially recovered during development

Figure S4. CPR5 Modulates Nucleocytoplasmic Transport of Stress-Related Cargo, Related to Figure 4

(A) Transient coexpression of mCherry-tagged NPR1/JAZ1/ABI5 with YFP-tagged WT (left panel) or G420D mutant (right panel) CPR5 in *N. benthamiana*.

(B) Quantification of results from experiments performed in (A). Localization of nuclear proteins in each cell was recorded as binomial data and categorized as 'nucleus only' or with significant 'cytosol retention'. A logistic regression model using CPR5/G420D as the sole independent variable can explain 95% of the data variance, illustrating the predominant effect of the functional CPR5 on protein nuclear transport.

(C) Phenotypes observed when *cpr5* was crossed with stress-related karyopherin and transport-related nucleoporin mutants.

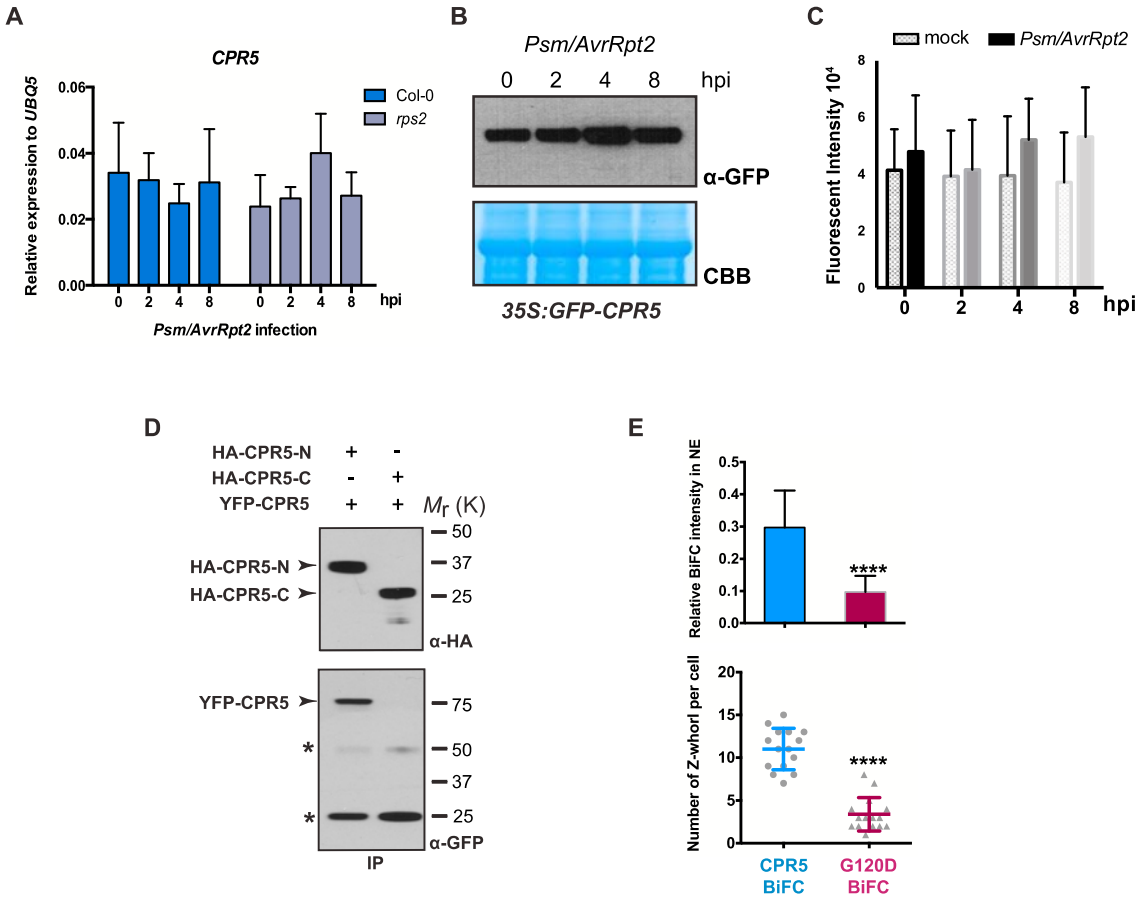

Figure S5. CPR5 Function Requires Homo-oligomerization, Related to Figure 5

(A) qRT-PCR determined relative expression levels of *CPR5* during ETI triggered by *Psm/AvrRpt2* at OD_{600nm} = 0.1. Samples were collected until 8 hr post inoculation (hpi) before ETI-induced PCD occurred. Data are presented as mean ± SDM (n = 3 biological replicates). Similar results were obtained in two independent experiments.

(B) GFP-CPR5 protein levels in *35S:GFP-CPR5* transgenic plants during ETI triggered by *Psm/AvrRpt2* at OD_{600nm} = 0.1 as measured by western blot using the GFP antibody.

(C) Fluorescence intensity measurement of GFP-CPR5 in the NE in *35S:GFP-CPR5* transgenic plants during ETI triggered by *Psm/AvrRpt2* at OD_{600nm} = 0.1. Data are presented as mean ± SDM (n = 15 cells for each time point and treatment).

(D) CPR5 homomeric interaction is mediated by its N-terminal domain. CPR5-N, rather than CPR5-C, mediated the homomeric interaction. In vitro pull-down assays were performed using wheat germ-synthesized recombinant proteins. Immunoprecipitation was performed using HA antibody-conjugated agarose beads. Immunoblotting was performed using GFP and HA antibodies. Stars indicate non-specific signals from immunoglobulins.

(E) The G120D mutation compromises heteromeric interactions of CPR5. BiFC was performed by transiently coexpressing nYFP-CPR5/cYFP-CPR5 or nYFP-G120D/cYFP-G120D in *N. benthamiana*. The BiFC intensity in the NE was normalized using averaged expression levels of YFP-CPR5/G120D measured in separate experiments and plotted as relative values (upper panel). Data are presented as mean ± SDM (n = 15 cells for each BiFC combination). The number of Z-whorl structures in each cell was measured when WT CPR5 or G120D mutant was transiently expressed in *N. benthamiana* (lower panel). Data are presented as mean ± SDM (n = 15 cells for each construct). Student's t test and non-parametric test were used, **** p-value < 0.0001.

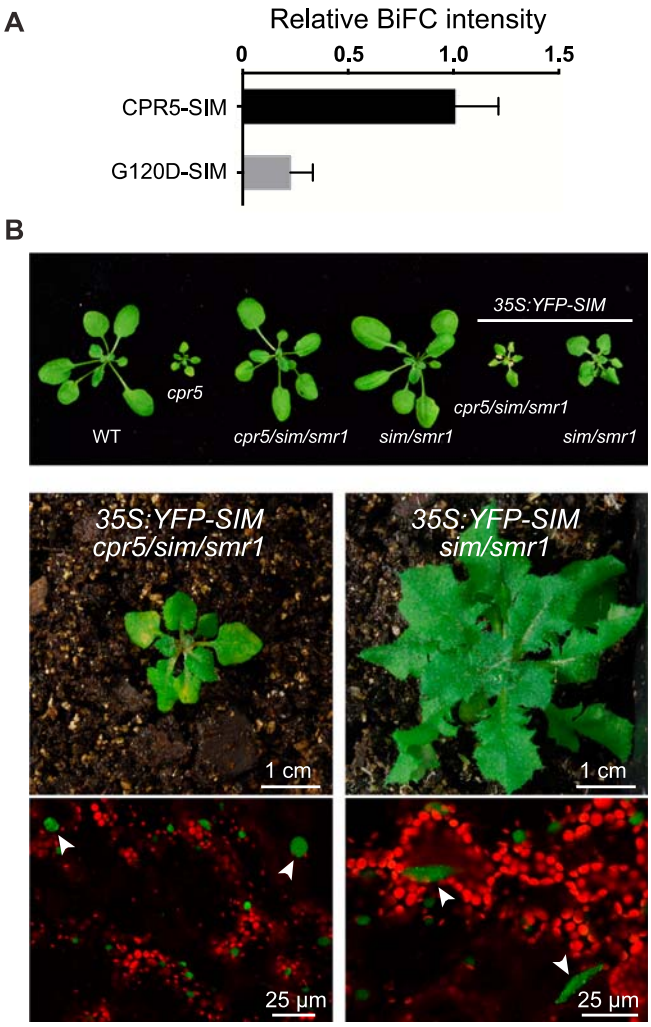

Figure S6. CKIs Release and NPC Transport Activity Change Are Both Required for ETI Activation, Related to Figure 6

(A) The G120D mutation compromises CPR5 interaction with SIM. BiFC was performed by transiently coexpressing SIM-nYFP and cYFP-CPR5/G120D in *N. benthamiana*. The BiFC intensity was normalized using averaged expression levels of YFP-CPR5/G120D measured in separate experiments. Data were plotted as relative values to the average BiFC intensity of CPR5-SIM and are presented as mean ± SDM (n = 15 cells for each BiFC combination).

(B) Three-week-old WT, *cpr5*, *sim smr1* and *cpr5 sim smr1* plants together with isogenic lines constitutively expressing YFP-SIM in *sim smr1*, and *cpr5 sim smr1* backgrounds (upper panel). Overexpression of SIM in the *sim smr1* background caused serrated leaf morphology without PCD, but in the *cpr5 sim smr1* background led to the *cpr5*-like dwarfism and PCD (lower panel). Nuclear YFP-SIM is pseudo-colored in green and chlorophyll autofluorescence is in red. Arrowheads indicate enlarged nuclei as a result of SIM overactivation (lower panel).